Energy Minimization Oriented Hybrid Semantic Data Transmission in Air-Ocean Integrated Networks: A Resource Allocation Design

Minghui Dai ⓘ, Tianshun Wang ⓘ, Shan Chang ⓘ, *Member, IEEE*, Zhou Su ⓘ, *Senior Member, IEEE*, and Yuan Wu ⓘ, *Senior Member, IEEE*

Abstract—With the development of new generation communication technologies, the future maritime information networks pave the way to promote the exploration of ocean resources. Moreover, the underwater data center (UDC) is considered to be a significant data storage and computing unit in future maritime networks for providing ocean services. However, the current deployment of UDC faces the critical issues, i.e., the long-distance underwater transmission is unreliable and the energy consumption and resources of underwater transmission are overloaded. To address the two critical issues of unreliable data transmission and high resource overheads, in this paper, we present a hybrid semantic data transmission architecture in air-ocean integrated networks, which can perceive the sea surface data accurately and transmit it to the UDC for processing. Specifically, in surface layer, uncrewed aerial vehicles (UAVs) perceive ocean environment and send data to the buoy via non-orthogonal multiple-access (NOMA) transmission to improve the channel utilization. In underwater layer, the buoy sends the collected data to UDC via semantic transmission, while the semantic fidelity metric is utilized to improve the transmission efficiency. A resource allocation problem for energy minimization is formulated to jointly optimize the semantic scaling factor, the NOMA decoding order, the communication and computing resource allocations. We exploit a decomposition approach to transform the problem into two sub-problems, where the optimal resource allocations are obtained by proposing efficient algorithms. Finally, we provide simulations to verify the effectiveness and efficiency of our proposed scheme. The results demonstrate that our proposal has the advantages of lower energy consumption compared to several baseline schemes.

Index Terms—Air-ocean integrated networks, hybrid semantic data transmission, energy efficiency, resource allocation.

I. INTRODUCTION

IN THE past decades, the development of next generation sensing and communication techniques (e.g., 6 G communications, integrated sensing and communication (ISAC)) enables human-beings to explore the ocean environment [1], [2], and the abundant maritime resources have attracted great interest from many researchers and industries to monitor and discover the oceans from multi-domain [3], [4]. For instance, offshore platforms are deployed for monitoring the maritime oil and mineral and obtaining the ocean information for researchers analysis. The development of maritime fisheries needs to be monitored in real-time to perceive the ocean environment (e.g., temperature, salinity, oil pollution) for shepherds decision-making. To this end, maritime resource exploration puts forward the new requirements for oceanic data sensing and collection, which is significant for researchers analysis and construction of smart oceans [5], [6]. However, unlike the terrestrial networks that can deploy a large number of stations, there is a severe lack of infrastructure in maritime networks due to the difficulty and harsh environment of deploying equipment, resulting in the limited ocean communication resources [7], [8]. Therefore, the ocean perception still faces the challenges of low sensing efficiency and high energy consumption.

Thanks to the development of uncrewed aerial vehicles (UAVs), various on-boards sensors (e.g., communication unit, sensing unit, computing unit) can be placed in UAVs for diverse applications. The high flexibility enables UAVs to be deployed in the air for ocean sensing and data transmission to buoys [9], [10]. For instance, UAVs can monitor the oil spill and send the warning information to offshore inspectors. Due to limited maritime communication resource, UAVs can assist the data transmission as the relay for surface nodes and ships. Therefore, the deployment of UAVs in ocean environment can promote many promising applications and services (e.g., navigation, rescuing). Although UAVs have the significant advantages in maritime sensing and data collection, the high energy consumption during data sensing and transmission is the critical issue that influences

the UAVs' endurance, which reduces the efficiency of maritime perception [11].

In underwater communication networks, the underwater acoustic channel suffers from low bandwidth and high bit error rate, which leads to low rate and unreliability for data transmission between maritime devices and underwater data center (UDC) [12], [13]. The growing amount of oceanic data requires high efficiency communication technique to support the data transmission. Semantic-aware communication, which is an emerging communication technology, has been regarded as an effective mode to significantly save the bandwidth and decrease the data transmission delay by extracting and delivering the semantic sensing data [14], [15]. However, in underwater transmission, the limited acoustic resource and the large amount of data cause the transmission congestion. Therefore, the semantic-aware communication puts forward the new requirement of semantic fidelity for oceanic data transmission [16].

There are some critical challenges that restrict the development of air-ocean integrated networks. On one hand, the high energy consumption and resources for oceanic data perception and transmission would lead to the reduced endurance of maritime devices. There have been some works studying the energy saving in maritime networks. The authors in [17] proposed an energy-efficient integrated framework to serve maritime applications with the assistance of intelligent autonomous underwater glider (AUG). The authors in [18] studied a reliable multi-source energy harvesting and management scheme for path-planning to support data transmission in underwater networks. Since maritime devices are generally powered by battery, it is difficult to recharge the battery. For instance, due to the limitation of on-board battery and computing capacity of UAVs, the semantic encoding of sensing data by UAVs can lead to high latency and consumption. This results in large encoding latency and reduces the endurance of UAVs for sensing ocean environment. Therefore, saving the energy consumption of maritime devices plays an important role in prolonging maritime services. On the other hand, the limited communication and computing resources in maritime environment result in the low resource utilization. A huge number of maritime nodes simultaneously accessing the same channel may cause the high interference and network congestion. Therefore, the resource allocation is a vital issue that should be addressed. There exist several works studying the resource allocation in maritime networks. The authors in [19] proposed a task offloading scheme and constructed a resource allocation problem aiming at minimizing the computational overhead of maritime devices. The authors in [20] investigated the uncrewed surface vehicles (USVs)-aided maritime wireless communications, with the objective of maximizing the throughput through optimizing the communication resource allocation. However, the joint energy consumption and resource allocation problem has not been studied for improving ocean services in maritime networks.

To address the above-mentioned issues, this paper presents a two-layer air-ocean integrated data collection framework consisting of the surface transmission and the underwater transmission, and proposes a hybrid semantic data transmission scheme to improve the accuracy of data collection and the reliability of data transmission. The objective is to minimize the system energy consumption via optimizing the maritime resource allocation. The main contributions of this work are summarized as follows.

- *Two-layer Air-Ocean Integrated Data Collection Framework:* Due to the lack of ocean infrastructure, we present a two-layer maritime data collection and transmission framework with the assistance of UAVs, which consists of the surface transmission layer and the underwater transmission layer. In the surface layer, UAVs are deployed over the surface to perceive oceanic data and transmit sensing data to the buoy. In the underwater layer, the buoy sends the collected data as the relay to the UDC for processing.

- *Hybrid Semantic Data Transmission Scheme:* To cope with the limited resources and improve the reliability of underwater data transmission in maritime networks, we propose a hybrid semantic data transmission scheme. In the surface layer, UAVs transmit their sensing data to the buoy via non-orthogonal multiple-access (NOMA) to improve the channel utilization and transmission throughput. In the underwater layer, the buoy sends the semantic data to the UDC through the semantic-based fidelity adjustment for saving the acoustic channel resource.

- *Energy-efficiency oriented Resource Allocation Design:* To prolong the endurance of maritime devices and save energy, we formulate a joint energy-efficiency and resource allocation problem for maritime data transmission. Despite the non-convex problem, we decompose it into two subproblems and obtain the optimal semantic scaling factor, the communication and computing resource allocation by the proposed algorithms. Simulation results demonstrate the effectiveness of the proposed scheme compared to other benchmark schemes.

This work is organized as follows. Section II studies the related works. Section III presents the system model and problem formulation. The problem transformation and proposed approach to solve the formulated problem are introduced in Section IV. Performance evaluation is illustrated in Section V. Section VI concludes this paper.

II. LITERATURE REVIEW

This section reviews the related works including the data collection and transmission scheme and the semantic-based data transmission scheme.

Data collection and transmission scheme: Cheng et al. [27] investigated the relay placement for underwater vehicle to forward data transmission while guaranteeing low latency and high reliability. Hu et al. [21] presented a secure data collection scheme in maritime Internet of Things, where the consensus algorithm is exploited to guarantee the integrity during data transmission. To reduce the workload of data collection on a single device, Han et al. [22] investigated autonomous underwater vehicle (AUV)-assisted cooperative task allocation and data collection scheme to reduce the delay and energy consumption of data collection. Liu et al. [28] studied the attenuation of age of information (AoI) during data collection, where the selected cluster heads are required to send the urgent data through multi-hop routing.

Su et al. [29] exploited USV-enabled data collection scheme from multiple maritime terminals, where the trajectory optimization problem is exploited to minimize the system consumption. Mcmahon et al. [30] proposed the trajectory optimization for the data collection of AUVs by considering the communication range constraints. Wen et al. [23] presented a multi-AUV path planning scheme to address the high data redundancy problem by using the reinforcement learning technology. Zong et al. [31] proposed a satellite-aided maritime monitoring framework to collect oceanic data, where a transmission scheme is exploited to improve the data transmission efficiency. Lyu et al. [32] investigated the data collection mechanism by considering the AoI in maritime systems, where the cooperative transmission scheme is proposed to improve the transmission efficiency. Qian et al. [24] studied the opportunistic route and full-duplex communication scheme for data collection and transmission in underwater sensor networks. Singhal et al. [33] studied the resource allocation scheme in dynamic spectrum access networks for improving the network performance. The above works study the underwater data sensing and collection schemes, and propose trajectory optimization algorithms for promoting data collection efficiency. Different from these discussed data collection and transmission works, this paper leverages the advantages of UAVs with high mobility and flexible deployment, and proposes the UAV-aided data sensing and collection scheme in air-ocean integrated networks.

Semantic-based data transmission scheme: Kadam et al. [25] formulated a data allocation optimization problem in semantic communication systems, where auto-encoder and auto-decoder are designed to extract the key information. Zhang et al. [34] studied semantic-based image transmission scheme, where the semantic encoding and data adaptation networks are considered for semantic transmission. Luong et al. [35] proposed a semantic-based edge communication system to compress the collected sensing data, where the deep learning algorithm is trained based on the valuation of the semantic symbol size. Li et al. [36] designed a dual-path for semantic encoder and decoder framework, where the image transmission task is executed to verify the performance of semantic communication system. Yang et al. [37] investigated the joint semantic information extraction and resource allocation scheme, aiming to minimize the system energy consumption. Zhang et al. [38] presented a novel multi-hop semantic transmission and communication system, where the recursive training approach is utilized for the encoder and decoder to solve the distortion accumulation problem. Ng et al. [39] investigated the resource allocation in semantic system in order to minimize the data size and reduce the energy consumption for data transmission. Mu et al. [26] studied the heterogeneous semantic-bit based communication networks, where the semantic similarity is constructed for evaluating the performance of semantic transmission. He et al. [40] formulated a multi-modal semantic communication framework, where the neural network is adopted for semantic encoder and decoder to extract different modalities information. Pu et al. [41] proposed the optimal resource allocation scheme for dynamic semantic mapping to improve the semantic spectral efficiency. Liu et al. [42] proposed the task-based semantic communication
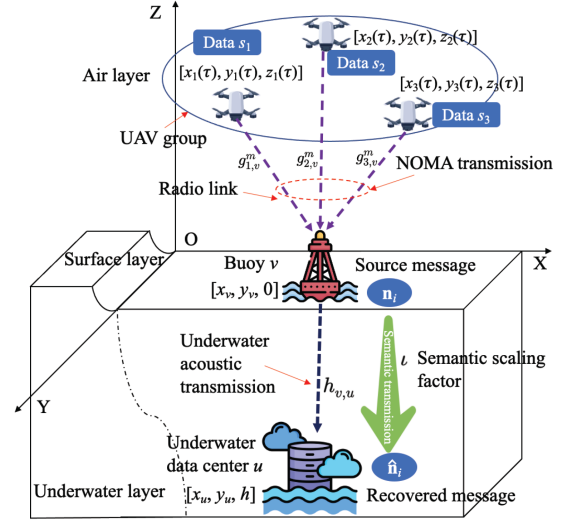

Fig. 1. System scenario of the hybrid semantic data transmission in air-ocean integrated networks.

scheme, in which the adaptable semantic compression approach is used to compress the extracted semantic information. The above works exploit semantic-based data transmission schemes, and propose resource allocation strategy. In contrast to the discussed semantic-based data transmission works above, this paper takes the limited acoustic channel into account and designs the semantic-based transmission scheme for improving the resource utilization and data transmission efficiency in air-ocean integrated networks. Moreover, a comparative analysis about semantic-based data transmission between our proposal and existing works is provided in Table I.

III. SYSTEM MODEL AND PROBLEM FORMULATION

This section presents the system model of hybrid semantic data transmission in air-ocean integrated networks. Then, the problem for the system energy consumption is formulated. Table II provides the main notations used in this paper.

A. System Model

As illustrated in Fig. 1, we consider the scenario of hybrid semantic data transmission in air-ocean integrated networks consisting of a UDC linked to offshore-station via fiber, a buoy equipped with edge computing units,[1] a group of UAVs denoted as $\mathcal{I} = \{1, \ldots, i, \ldots, I\}$. UAVs sense ocean environment and transmit data to the buoy via wireless radio links. The buoy then sends data to the UDC based on semantic transmission via acoustic links. The subscript "u" is utilized to denote the UDC, and "v" is used to denote the buoy. The proposed framework is comprised of four phases. Phase I is the NOMA-aided data uploading from UAVs to the buoy. Phase II is the semantic fidelity-adjustment for the received data and semantic encoding at the buoy. Phase III is the underwater acoustic semantic transmission. Phase IV is the semantic decoding at the UDC. Specifically, multiple UAVs

---

[1]The buoy has powerful computing units, which can be deployed on the surface for facilitating computing with low latency.

TABLE I
COMPARATIVE ANALYSIS FOR SEMANTIC-BASED DATA TRANSMISSION

Ref	Topic focus on	Performance Metric	Functionality	Pros	Cons	Complexity	CMST[1]
[21]	Underwater networks	Minimize energy consumption	Data collection and storage	Secure and privacy preservation	High deployment cost	High	✗
[22]	Underwater acoustic sensor networks	Optimize path planning	Task allocation &data collection	Real-time scheduling	Increased energy consumption	High	✗
[23]	Underwater wireless networks	Maximize system efficiency	Data collection Trajectory optimization	High communication efficiency	High data redundancy	High	✗
[24]	Underwater sensor networks	Opportunistic route planning	Data transmission	Reliable and efficient transmission	High signal interference	Medium	✗
[25]	Semantic communication system	Minimize average data transmission	Data allocation semantic transmission	Improved transmission accuracy	Increased energy consumption	High	✗
[26]	Semantic-bit communication system	Maximize semantic-rate	Hybrid semantic-bit transmission	Flexible transmission strategy	Limited system resources	High	✗
Our proposal	Air-ocean semantic communication	Minimize system energy consumption	Hybrid data collection &semantic transmission	Lightweight semantic transmission system	High energy consumption	Low	✓

[1] "CMST" means "Customized for Marine Semantic Transmission" (customized to meet the requirements of marine semantic transmission).

TABLE II
KEY NOTATIONS USED IN THIS PAPER

Notation	Definition	Notation	Definition
$\gamma_{i,v}^m$	The received SINR from UAV i to the buoy.	$\varrho_{i,v}$	The computing resource allocated to encode the message $\mathbf{n}_i$ at the buoy.
$r_{i,v}^m$	The data throughput from UAV i to the buoy.	$t_{i,v}^{\text{enc}}$	The computation time of semantic encoding at the buoy.
$p_{i,v}^m$	The transmission power of UAV i to the buoy.	$E_{i,v}^{\text{enc}}$	The energy consumption for encoding the message.
$g_{i,v}^m$	The channel power gain from UAV i to the buoy.	$\phi(d_{v,u},\lambda)$	The attenuation of underwater acoustic signals.
$d_{i,v}$	The distance between UAV i and the buoy.	$\chi_{v,u}$	The received SINR at the buoy.
$t_{i,v}^m$	The transmission time of UAV i to the buoy.	$t_{i,v}^m$	The transmission time of UAV i to the buoy.
s_i	The data size required to transmit to the buoy.	t_i^{tran}	The semantic transmission time.
E_i^m	The transmission energy consumption of UAV i to the buoy.	E_i^{tran}	The energy consumption of semantic transmission.
ι	The semantic scaling factor.	$\varrho_{i,u}$	The computing resource allocated to decode the message $\mathbf{n}_i$ at the UDC.
$\mathbf{n}_i$	The message of collected source data by UAV i.	$t_{i,u}^{\text{dec}}$	The computation time of semantic decoding.
$\mathbf{x}_i$	The semantic symbol at the transmitter side.	$E_{i,u}^{\text{dec}}$	The energy consumption for decoding message.
$\mathbf{y}_i$	The received signal at the UDC.	T_i^{tot}	The total latency for data transmission.
$\varphi_i^\iota(\mathbf{n}_i;\widehat{\mathbf{n}}_i)$	The semantic similarity metric.	E^{tot}	The total energy consumption for data transmission.

cooperatively perceive ocean environment and group a NOMA cluster to send sensing data to the buoy via radio links. The buoy is responsible for semantically compressing data based on the semantic fidelity-adjustable model (which is illustrated in Phase II). The UDC receives the encoded semantic data and then decodes the data for analysis.

Phase I. NOMA-aided Data Uploading Between UAVs and Buoy: To improve the spectrum efficiency, the NOMA is adopted as the multi-access scheme for data transmission between UAVs and buoy. According to [43], we use $\mathbf{o}^m$ to denote the decoding order at the buoy, where the index $m \in \{1, 2, \ldots, i!, \ldots, I!\}$. Here, $\mathbf{o}^m(i)$ indicates the decoding order of UAV i under the m-th decoding order $\mathbf{o}^m$ via the successive interference cancellation (SIC) technology at the buoy.[2] Let $p_{i,v}^m$ denote the transmission power of UAV i to the buoy under the m-th decoding-ordering $\mathbf{o}^m$. The channel power gain from UAV i to the buoy under the m-th decoding-order $\mathbf{o}^m$ is denoted as $g_{i,v}^m$. Thus, given the decoding order $\mathbf{o}^m$, the received signal-to-interference-plus-noise

ratio (SINR) from UAV i to the buoy can be denoted as

$$\gamma_{i,v}^m = \frac{p_{i,v}^m g_{i,v}^m}{\sum_{j \in \mathcal{I}, \mathbf{o}^m(j) < \mathbf{o}^m(i)} p_{j,v}^m g_{j,v}^m + N_v}, \forall i \in \mathcal{I}, \quad (1)$$

and the data throughput from UAV i to the buoy can be expressed as

$$r_{i,v}^m = W \log_2\left(1 + \gamma_{i,v}^m\right), \forall i \in \mathcal{I}, \quad (2)$$

where parameter W denotes the uplink channel bandwidth. Parameter N_v means the additive Gaussian noise at the buoy. The channel power gain between UAVs and buoy under the m-th decoding-order $\mathbf{o}^m$ can be modeled as the Line-of-Sight (LoS) link, denoted as

$$g_{i,v}^m = \alpha d_{i,v}^{-\sigma}, \forall i \in \mathcal{I}, \quad (3)$$

where α means the channel power gain. σ is the path loss exponent. $d_{i,v}$ is the distance between UAV i and the buoy.

We use a 3-D Cartesian coordinate to measure the locations of UAVs. We denote the position of buoy v as $\mathbf{Q}_v = [x_v, y_v, 0] \in \mathbb{R}^{3 \times 1}$. We use T^{ser} to indicate the service duration of UAVs, and the duration are divided into N equal-length time slot $\jmath$ and $N = T^{\text{ser}}/\jmath$. During each time slot, the positions of UAVs remain unchanged. The time-varying horizontal

---

[2]Considering the powerful computing units of buoy, and NOMA can accommodate an arbitrary decoding order at the buoy. The NOMA decoding delay at the buoys can be ignored compared to the data transmission delay. Thus, our modelings can be applicable to large-scale air-ocean integrated networks by increasing the numbers of UAVs, buoys and UDCs.

coordinate is taken into account, the position of UAV i is denoted as $\mathbf{Q}_i = [x_i(\jmath), y_i(\jmath), z_i(\jmath)] \in \mathbb{R}^{3 \times 1}, \forall i \in \mathcal{I}$. For each UAV i within a time slot, the mobility constraint satisfies $\| \mathbf{Q}_i(\jmath + 1) - \mathbf{Q}_i(\jmath) \|^2 \leq (\jmath V_i^{\max})^2, \forall i \in \mathcal{I}$, where $V_i^{\max}$ means the maximum sailing speed of UAV i. To ensure the channel quality of data transmission, the distance between UAV i and buoy v satisfies

$$\| \mathbf{Q}_i(\jmath) - \mathbf{Q}_v \| \leq \daleth^{\max}, \forall i \in \mathcal{I}, \qquad (4)$$

where $\daleth^{\max}$ means the maximum communication distance between UAV i and buoy v.

We use s_i to denote the data size required to transmit to the buoy. Thus, the transmission time of UAV i to the buoy under the given decoding order $\mathbf{o}^m$ can be expressed as

$$t_{i,v}^m = \frac{s_i}{r_{i,v}^m}, \forall i \in \mathcal{I}. \qquad (5)$$

The transmission energy consumption of UAV i to buoy under the given decoding order $\mathbf{o}^m$ can be expressed as

$$E_i^m = p_{i,v}^m t_{i,v}^m = \frac{p_{i,v}^m s_i}{r_{i,v}^m}, \forall i \in \mathcal{I}. \qquad (6)$$

Phase II. Semantic Encoding based on Fidelity Metric in Buoy: After receiving the collected data from UAVs, the buoy will decode the data signal of each UAV via SIC. Due to the limited underwater communication resource, we introduce the semantic fidelity adjustable model for underwater transmission to satisfy diverse requirements. We use $\mathbf{n}_i$ to denote the message of collected source data s_i by UAV i, and use $\iota(\iota \in [0, 1])$ to denote the semantic scaling factor for fidelity adjustment.

First, at the transmitter side, the buoy is responsible for extracting and encoding the semantic information of the received message $\mathbf{n}_i$. Thus, the corresponding semantic symbol can be expressed as

$$\mathbf{x}_i = f_v(\mathbf{n}_i; \mathbf{\Theta}^\iota), \forall i \in \mathcal{I}, \qquad (7)$$

where $f_v(\cdot; \mathbf{\Theta}^\iota)$ means the semantic encoding function with the weighting parameter $\mathbf{\Theta}$ at the buoy.

Second, the buoy transmits the extracted semantic to the UDC via acoustic channel. The received signal at the UDC can be expressed as

$$\mathbf{y}_i = h_{v,u} \mathbf{x}_i + N_u, \forall i \in \mathcal{I}, \qquad (8)$$

where $h_{v,u}$ denotes the underwater acoustic channel gain between buoy v and UDC u. The value of $h_{v,u}$ is illustrated in Phase III. N_u means the additive ocean noise at the UDC u.

Third, at the receiver side, the received semantic information is fed to the UDC for decoding. The decoded message can be expressed as

$$\hat{\mathbf{n}}_i = f_u^{-1}(\mathbf{y}_i; \mathbf{\Phi}^\iota), \forall i \in \mathcal{I}, \qquad (9)$$

where $f_u^{-1}(\cdot; \mathbf{\Phi}^\iota)$ indicates the semantic decoding function with the weighting parameter $\mathbf{\Phi}$ at the UDC.

Given a semantic scaling factor ι and the full-size semantic encoder and decoder $\{\mathbf{\Theta}, \mathbf{\Phi}\}$, we aim to obtain a pair of small-size semantic encoder and decoder $\{\mathbf{\Theta}^\iota, \mathbf{\Phi}^\iota\}$. In specific,

the semantic model derivation is conducted based on a layer-by-layer manner. Regarding a pre-determined convolution layer with several filters ϕ (i.e., the width of the layer), we can choose the weights of the first filters $\iota \phi$ to build the layer for a small-size semantic model.

Based on [44], [45], in order to quantitatively characterize the semantic accuracy between the source message $\mathbf{n}_i$ and the recovered message $\hat{\mathbf{n}}_i$, we introduce the semantic fidelity metric, which can be quantified by the cosine similarity as

$$\varphi_i^\iota(\mathbf{n}_i; \hat{\mathbf{n}}_i) = \frac{S^\iota(\mathbf{n}_i) S^\iota(\hat{\mathbf{n}}_i)^\mathrm{T}}{\| S^\iota(\mathbf{n}_i) \| \| S^\iota(\hat{\mathbf{n}}_i) \|}, \forall i \in \mathcal{I}, \qquad (10)$$

where $S^\iota(\cdot)$ is the pre-trained model with the semantic scaling factor ι. The training objective is to minimize the error of data reconstruction. We use $l(e, \hat{e})$ to denote the pre-determined loss function with the dataset $\Re^{\mathrm{set}}$. The learning objective can be denoted as $\min_{\mathbf{\Theta}, \mathbf{\Phi}} \int_{\iota^{\min}}^1 \sum_{e \in \Re^{\mathrm{set}}} l(e, f(e; \mathbf{\Theta}, \mathbf{\Phi}, \iota)) d\iota$, where $f(\cdot)$ denotes the function of calculating the reconstructed data. $\varphi_i^\iota(\mathbf{n}_i; \hat{\mathbf{n}}_i) \in [0, 1]$ denotes the semantic fidelity of the recovered message. If $\varphi_i^\iota(\mathbf{n}_i; \hat{\mathbf{n}}_i)$ takes the value 1, it means the highest similarity between the source message $\mathbf{n}_i$ and the recovered message $\hat{\mathbf{n}}_i$, while the value 0 means that there is no similarity. The relationship between semantic fidelity $\varphi_i^\iota(\mathbf{n}_i; \hat{\mathbf{n}}_i)$ and the scaling factor ι can be expressed as

$$\varphi_i^\iota(\mathbf{n}_i; \hat{\mathbf{n}}_i) = \omega_1 \ln\left(\frac{\omega_2}{\iota} + \omega_3\right) + \omega_4, \forall i \in \mathcal{I}, \qquad (11)$$

where $\omega_1, \omega_2, \omega_3, \omega_4$ are the hyper-parameters. Eq (11) indicates that the semantic fidelity can be adjusted flexibly via the scaling factor. In the following, we use φ_i^ι to replace $\varphi_i^\iota(\mathbf{n}_i; \hat{\mathbf{n}}_i)$ for convenience.

For semantic encoding, we use B_i to denote the computation workload for encoding the message $\mathbf{n}_i$ at the buoy. With the semantic scaling factor ι, the encoding workload at the buoy can be expressed as $\iota^2 B_i$ [46], [47]. The computation time of semantic encoding at the buoy can be denoted as

$$t_{i,v}^{\mathrm{enc}} = \frac{\iota^2 B_i}{\varrho_{i,v}}, \forall i \in \mathcal{I}, \qquad (12)$$

where $\varrho_{i,v}$ denotes the computing resource allocated to encode the message $\mathbf{n}_i$ at the buoy. The power consumption of buoy for encoding message $\mathbf{n}_i$ is $p_{i,v}^{\mathrm{enc}} = \epsilon \varrho_{i,v}^3$, where parameter ϵ denotes the energy coefficient depending on the chip architecture. Thus, the energy consumption for encoding the message $\mathbf{n}_i$ at the buoy can be expressed as

$$E_{i,v}^{\mathrm{enc}} = p_{i,v}^{\mathrm{enc}} t_{i,v}^{\mathrm{enc}} = \epsilon \varrho_{i,v}^2 \iota^2 B_i, \forall i \in \mathcal{I}. \qquad (13)$$

Phase III. Underwater Acoustic Semantic Transmission Between Buoy and UDC: Due to the high packet loss rate and high channel attenuation of radio link in underwater transmission, we consider the acoustic semantic transmission between buoy (semantic transmitter) and UDC (semantic receiver). Let λ denote the frequency of the acoustic signal, we can express the acoustic channel gain between buoy and UDC as

$$h_{v,u} = \frac{1}{\hat{W} N_u \phi(d_{v,u}, \lambda)}, \qquad (14)$$

where $\hat{W}$ denotes the acoustic bandwidth. $\phi(d_{v,u}, \lambda)$ means the attenuation of underwater acoustic signals. According to [48], $\phi(d_{v,u}, \lambda)$ is related to the frequency of the acoustic signal λ and the distance $d_{v,u}$ between buoy v and UDC u and it can be expressed as

$$\phi\left(d_{v,u}, \lambda\right) = \xi_0(d_{v,u})^{\beta} \mathcal{A}(\lambda)^{d_{v,u}}, \tag{15}$$

where ξ_0 means a unit-normalizing constant. β is a constant parameter. We use $\mathbf{Q}_u = [\overline{x}_u, \overline{y}_u, h] \in \mathbb{R}^{3 \times 1}$ to denote the position of UDC u. Here, h denotes the vertical distance between the seabed and surface. The distance between buoy v and UDC u can be expressed as

$$d_{v,u} = \sqrt{(x_v - \overline{x}_u)^2 + (y_v - \overline{y}_u)^2 + h^2}. \tag{16}$$

The absorption coefficient $\mathcal{A}(\lambda)$ can be calculated by [49]

$$\begin{aligned} 10 \log \mathcal{A}\left(\lambda\right) &= \frac{0.11\lambda^2}{1 + \lambda^2} + \frac{44\lambda^2}{4100 + \lambda^2} \\ &\quad + 2.75e^{-4}\lambda^2 + 0.003. \end{aligned} \tag{17}$$

Based on the above analysis, we use p_v to denote the transmission power of buoy v. Then, the received SINR at the UDC for transmitting message $\mathbf{n}_i$ can be expressed as

$$\chi_{v,u} = \frac{p_v h_{v,u}}{N_u}, \tag{18}$$

and the data rate from the buoy to the UDC can be expressed as

$$r_{v,u} = \hat{W} \log_2\left(1 + \chi_{v,u}\right). \tag{19}$$

For semantic transmission, we use Q_i to denote the size of semantic information for message $\mathbf{n}_i$. With the semantic scaling factor ι, the semantic size for transmitting is ιQ_i. Thus, the semantic transmission time for message $\mathbf{n}_i$ can be denoted by

$$t_i^{\text{tran}} = \frac{\iota Q_i}{r_{v,u}}, \forall i \in \mathcal{I}. \tag{20}$$

The transmission energy consumption of message $\mathbf{n}_i$ can be denoted as

$$E_i^{\text{tran}} = p_v t_i^{\text{tran}} = \frac{\iota Q_i p_v}{r_{v,u}}, \forall i \in \mathcal{I}. \tag{21}$$

Phase IV. Semantic Decoding in the UDC: For semantic decoding, we use D_i to denote the computing workload for decoding the message $\mathbf{n}_i$ at the UDC. With the semantic scaling factor ι, the decoding workload at the UDC is $\iota^2 D_i$. The computation time of semantic decoding at the UDC can be expressed as

$$t_{i,u}^{\text{dec}} = \frac{\iota^2 D_i}{\varrho_{i,u}}, \forall i \in \mathcal{I}, \tag{22}$$

where $\varrho_{i,u}$ denotes the computing resource allocated to decode the message $\mathbf{n}_i$ at the UDC. The power consumption of UDC for decoding message $\mathbf{n}_i$ is $p_{i,u}^{\text{dec}} = \epsilon \varrho_{i,u}^3$. Thus, the energy consumption for decoding the message $\mathbf{n}_i$ at the UDC can be expressed as

$$E_{i,u}^{\text{dec}} = p_{i,u}^{\text{dec}} t_i^{\text{dec}} = \epsilon \varrho_{i,u}^2 \iota^2 D_i, \forall i \in \mathcal{I}. \tag{23}$$

Based on the above modeling, the total delay and the total energy consumption in the four phases can be separately calculated by

$$\begin{aligned} T_i^{\text{tot}} &= t_{i,v}^m + t_{i,v}^{\text{enc}} + t_i^{\text{tran}} + t_{i,u}^{\text{dec}} \\ &= \frac{s_i}{r_{i,v}^m} + \frac{\iota^2 B_i}{\varrho_{i,v}} + \frac{\iota Q_i}{r_{v,u}} + \frac{\iota^2 D_i}{\varrho_{i,u}}, \forall i \in \mathcal{I}. \end{aligned} \tag{24}$$

$$\begin{aligned} E^{\text{tot}} &= \sum_{i=1}^{I} \left(E_i^m + E_{i,v}^{\text{enc}} + E_i^{\text{tran}} + E_{i,u}^{\text{dec}} \right) \\ &= \sum_{i=1}^{I} \left(\frac{p_{i,v}^m s_i}{r_{i,v}^m} + \epsilon \varrho_{i,v}^2 \iota^2 B_i + \frac{\iota Q_i p_v}{r_{v,u}} + \epsilon \varrho_{i,u}^2 \iota^2 D_i \right). \end{aligned} \tag{25}$$

B. Problem Formulation

In our considered scenario, we aim to minimize the system energy consumption of data transmission by jointly optimizing the SIC ordering $\mathbf{o}^m$ in Phase I, transmission power $p_{i,v}^m$, p_v in Phase I and Phase III, semantic fidelity strategy ι in Phase II, and computing resource allocation $\varrho_{i,v}$, $\varrho_{i,u}$ in Phase II and Phase IV. The mathematical problem is formulated as follows ("SEC" means "System Energy Consumption")

$$(\text{SEC}): \min E^{\text{tot}}$$

$$\text{subject to}: 0 \leq \sum_{i=1}^{I} \varrho_{i,v} \leq \varrho_v^{\max}, \varrho_{i,v} \geq 0, \tag{26}$$

$$0 \leq \sum_{i=1}^{I} \varrho_{i,u} \leq \varrho_u^{\max}, \varrho_{i,u} \geq 0, \tag{27}$$

$$0 \leq p_{i,v}^m \leq P^{\max}, \forall i \in \mathcal{I}, \tag{28}$$

$$0 \leq p_v \leq P^{\max}, \tag{29}$$

$$0 \leq \iota \leq 1, \tag{30}$$

$$\varphi^{\min} \leq \varphi_i^{\iota}, \forall i \in \mathcal{I}, \tag{31}$$

$$0 \leq T_i^{\text{tot}} \leq T^{\max}, \forall i \in \mathcal{I},$$

$$\text{variables}: \mathbf{o}^m, p_{i,v}^m, p_v, \varrho_{i,v}, \varrho_{i,u}, \iota, \forall i \in \mathcal{I}. \tag{32}$$

In Problem (SEC), constraints (26) and (27) mean that the allocated computation resource of buoy and UDC cannot exceed the maximum capacity $\varrho_v^{\max}$ and $\varrho_u^{\max}$, respectively. Constraints (28) and (29) guarantee that the transmission power of UAV and buoy cannot be higher than the maximum power $P^{\max}$. Constraints (30) and (31) indicate that the semantic fidelity should be higher than the lower bound $\varphi^{\min}$. Constraint (32) ensures that the data transmission delay cannot be larger than the maximum tolerable latency $T^{\max}$.

Due to the existence of SIC ordering variable, it can be found that Problem (SEC) is a mixed integer nonlinear optimization, which is difficult to solve. In the following, we transform the original problem into a convex optimization by fixing the SIC ordering, and exploit a layered structure to solve it.

IV. PROBLEM TRANSFORMATION AND PROPOSED APPROACH TO SOLVE PROBLEM (SEC)

In this section, we first simplify the formulated problem. Then, we formulate a layered decomposition approach to address the formulated problem.

A. Problem Transformation

By analyzing Problem (SEC), we derive the following proposition.

Proposition 1: The optimal solutions $\mathbf{o}^{m,*}$, $p_{i,v}^{m,*}$, p_v^*, $\varrho_{i,v}^*$, $\varrho_{i,u}^*$, ι^* of Problem (SEC) are achieved when the equality always holds (i.e., $\varphi_i^{\iota} = \varphi^{\min}$ and $T_i^{\text{tot},*} = T^{\max}$) for constraints (31) and (32).

Proof: The contradiction approach is adopted to prove Proposition 1. We assume that there exists another solution $\varrho_{i,v}' < \varrho_{i,v}^*$ such that $T_i^{\text{tot},'} < T^{\max}$ and $E^{\text{tot},'} < E^{\text{tot},*}$, where $T_i^{\text{tot},'}$ and $E^{\text{tot},'}$ denote the corresponding total latency and total energy consumption under the new solution $\varrho_{i,v}'$. Based on (24), it can be found that $T_i^{\text{tot},'}$ is decreasing with the increase of $\varrho_{i,v}'$. We can obtain $\varrho_{i,v}' > \varrho_{i,v}^*$ under the condition $T_i^{\text{tot},'} < T^{\max}$. Moreover, since $E^{\text{tot},*}$ is increasing with the increase of $\varrho_{i,v}^*$ based on (25), we can obtain $E^{\text{tot},'} > E^{\text{tot},*}$ under the condition $\varrho_{i,v}' > \varrho_{i,v}^*$. This contradicts to the assumption. Therefore, there does not exist the solution $\varrho_{i,v}'$. The result also applies for $\varphi^{\min} \leq \varphi_i^{\iota}$. This completes our proof. ■

Proposition 1 enables us to obtain the optimal semantic scaling factor by letting $\varphi_i^{\iota} = \varphi^{\min}$, which can be expressed as

$$\iota^* = \frac{\omega_2}{e^{\frac{\varphi^{\min} - \omega_4}{\omega_1}} - \omega_3}. \quad (33)$$

Next, we transform Problem (SEC) into convexity via reparametrization. Through transforming (1), the required transmission power $p_{i,v}^m$ of UAV i can be denoted as

$$p_{i,v}^m = \frac{N_v}{g_{i,v}^m} \gamma_{i,v}^m \prod_{j \in \mathcal{I}, \mathbf{o}^m(j) < \mathbf{o}^m(i)} \left(1 + \gamma_{j,v}^m\right), \forall i \in \mathcal{I}. \quad (34)$$

Therefore, constraint (28) can be rewritten as

$$0 \leq \frac{N_v}{g_{i,v}^m} \gamma_{i,v}^m \prod_{j \in \mathcal{I}, \mathbf{o}^m(j) < \mathbf{o}^m(i)} \left(1 + \gamma_{j,v}^m\right) \leq P^{\max},$$
$$\forall i \in \mathcal{I}. \quad (35)$$

With loss of optimality, the optimal solutions are always achieved when the data throughput in (2) satisfies

$$r_{i,v}^m \leq W \log_2\left(1 + \gamma_{i,v}^m\right), \forall i \in \mathcal{I}. \quad (36)$$

By transforming (18), the required transmission power p_v can be expressed as

$$p_v = \frac{\chi_{v,u} N_u}{h_{v,u}}. \quad (37)$$

Then, constraint (29) can be rewritten as

$$0 \leq \frac{\chi_{v,u} N_u}{h_{v,u}} \leq P^{\max}. \quad (38)$$

Moreover, at the optimal point, the data rate of buoy satisfies

$$r_{v,u} \leq \hat{W} \log_2\left(1 + \chi_{v,u}\right). \quad (39)$$

Based on the above transformation, given the SIC ordering, we denote the equivalent form of Problem (SEC) as

$$\text{(SEC-E)}: \min \sum_{i=1}^{I} \left\{ \frac{s_i N_v}{r_{i,v}^m g_{i,v}^m} \gamma_{i,v}^m \prod_{j \in \mathcal{I} \mathbf{o}^m(j) < \mathbf{o}^m(i)} \left(1 + \gamma_{j,v}^m\right) \right.$$
$$+ \frac{Q_i \chi_{v,u} N_u}{r_{v,u} h_{v,u}} \left(\frac{\omega_2}{e^{\frac{\varphi^{\min} - \omega_4}{\omega_1}} - \omega_3} \right)$$
$$\left. + \epsilon \left(B_i \varrho_{i,v}^2 + D_i \varrho_{i,u}^2\right) \left(\frac{\omega_2}{e^{\frac{\varphi^{\min} - \omega_4}{\omega_1}} - \omega_3} \right)^2 \right\}$$

subject to : constraints (26), (27), (35), (36), (38), (39),
$$r_{i,v}^m \geq 0, \gamma_{i,v}^m \geq 0, r_{v,u} \geq 0, \chi_{v,u} \geq 0,$$
$$T_i^{\text{tot}} = T^{\max}, \forall i \in \mathcal{I},$$

variables : $r_{i,v}^m, \gamma_{i,v}^m, r_{i,u}, \chi_{i,u}, \varrho_{i,v}, \varrho_{i,u}, \forall i \in \mathcal{I}$.

Next, we study the convexity characteristic of the equivalent Problem (SEC-E).

Proposition 2: Problem (SEC-E) can be transformed into a convex form.

Proof: Let $\hat{r}_{i,v}^m$, $\hat{\gamma}_{i,v}^m$, $\hat{r}_{v,u}$, $\hat{\chi}_{v,u}$, $\hat{\varrho}_{i,v}$, $\hat{\varrho}_{i,u}$ denote the logarithmic transformation regarding the variables $r_{i,v}^m$, $\gamma_{i,v}^m$, $r_{v,u}$, $\chi_{v,u}$, $\varrho_{i,v}$, $\varrho_{i,u}$, respectively. We can obtain $\hat{r}_{i,v}^m = \log r_{i,v}^m$, $\hat{\gamma}_{i,v}^m = \log \gamma_{i,v}^m$, $\hat{r}_{v,u} = \log r_{v,u}$, $\hat{\chi}_{v,u} = \log \chi_{v,u}, \hat{\varrho}_{i,v} = \log \varrho_{i,v}, \hat{\varrho}_{i,u} = \log \varrho_{i,u}$. Therefore, through the logarithmic domain transformation, the objective function of Problem (SEC-E) can be expressed by (40) shown at the bottom of the next page. With the logarithmic domain transformation, it can be obtained that the transformed objective function $\hat{E}^{\text{tot}}$ is a convex function.

Next, we prove that each constraint in Problem (SEC-E) is the convex constraint via the logarithmic domain transformation. Constraints (26) and (27) can be rewritten as follows

$$\log \left(\sum_{i=1}^{I} e^{\hat{\varrho}_{i,v}} \right) \leq \log \varrho_v^{\max}, \quad (41)$$

$$\log \left(\sum_{i=1}^{I} e^{\hat{\varrho}_{i,u}} \right) \leq \log \varrho_u^{\max}, \quad (42)$$

respectively. It can be found that the logarithmic transformation of constraints (41) and (42) is convex.

For the transmission power, constraints (35) and (38) can be rewritten as

$$\hat{\gamma}_{i,v}^m + \sum_{j \in \mathcal{I}, \mathbf{o}^m(j) < \mathbf{o}^m(i)} \log \left(1 + e^{\hat{\gamma}_{j,v}^m}\right) \leq \log \frac{P^{\max} g_{i,v}^m}{N_v},$$
$$\forall i \in \mathcal{I}, \quad (43)$$

$$\hat{\chi}_{v,u} \leq \log \frac{P^{\max} h_{v,u}}{N_u}, \quad (44)$$

respectively. We find that constraints (43) and (44) are convex.

For the data throughput, constraints (36) and (39) can be rewritten as

$$\hat{r}_{i,v}^m \leq \log\left(W\log_2\left(1 + e^{\hat{\gamma}_{i,v}^m}\right)\right), \forall i \in \mathcal{I}, \tag{45}$$

$$\hat{r}_{v,u} \leq \log\left(\hat{W}\log_2\left(1 + e^{\hat{\chi}_{v,u}}\right)\right), \tag{46}$$

respectively. Since the right items of inequality constraints (45) and (46) are concave function, constraints (45) and (46) are convex.

For the data transmission delay, we can express the delay constraint as follows

$$\log\left\{\begin{array}{l} s_i e^{-\hat{r}_{i,v}^m} + Q_i e^{-\hat{r}_{v,u}}\left(\dfrac{\omega_2}{e^{\frac{\varphi^{\min}-\omega_4}{\omega_1}}-\omega_3}\right) \\ + \left(\dfrac{\omega_2}{e^{\frac{\varphi^{\min}-\omega_4}{\omega_1}}-\omega_3}\right)^2 \left(B_i e^{-\hat{\varrho}_{i,v}} + D_i e^{-\hat{\varrho}_{i,u}}\right) \end{array}\right\} \tag{47}$$
$$= \log T^{\max}, \forall i \in \mathcal{I}.$$

It can be found that constraint (47) is convex.

Therefore, with the logarithmic domain transformation, Problem (SEC-E) is transformed into a convex problem. This completes our proof. ∎

Based on Proposition 2, we can rewrite the convex optimization problem regarding Problem (SEC-E) as follows

(SEC-C) : $\min \hat{E}^{\text{tot}}$

subject to : constraints (41), (42), (43), (44), (45), (46), (47),

variables : $\hat{r}_{i,v}^m, \hat{\gamma}_{i,v}^m, \hat{r}_{v,u}, \hat{\chi}_{v,u}, \hat{\varrho}_{i,v}, \hat{\varrho}_{i,u}$.

To this end, given the SIC ordering in the NOMA transmission phase, we transform the original problem into a convex optimization. Therefore, this feature enables us to solve the original problem through decomposition approach. Specifically, we decompose Problem (SEC) into two sub-problems: (Sub-I) for resource allocation optimization $\hat{r}_{i,v}^m, \hat{\gamma}_{i,v}^m, \hat{r}_{v,u}, \hat{\chi}_{v,u}, \hat{\varrho}_{i,v}, \hat{\varrho}_{i,u}$, and (Sub-II) for SIC ordering optimization $\mathbf{o}^m$. Fig. 2 shows the decomposition process for solving the original Problem (SEC).

- (Sub-I) for resource allocation optimization. Given the SIC ordering $\mathbf{o}^m$, we aim to solve the resource allocation $\hat{r}_{i,v}^m$, $\hat{\gamma}_{i,v}^m, \hat{r}_{v,u}, \hat{\chi}_{v,u}, \hat{\varrho}_{i,v}, \hat{\varrho}_{i,u}$, which leads to the following problem

(SEC-Sub-I) : $\min \hat{E}^{\text{tot}}$

subject to : constraints (41), (42), (43), (44), (45),

constraints (46), (47),

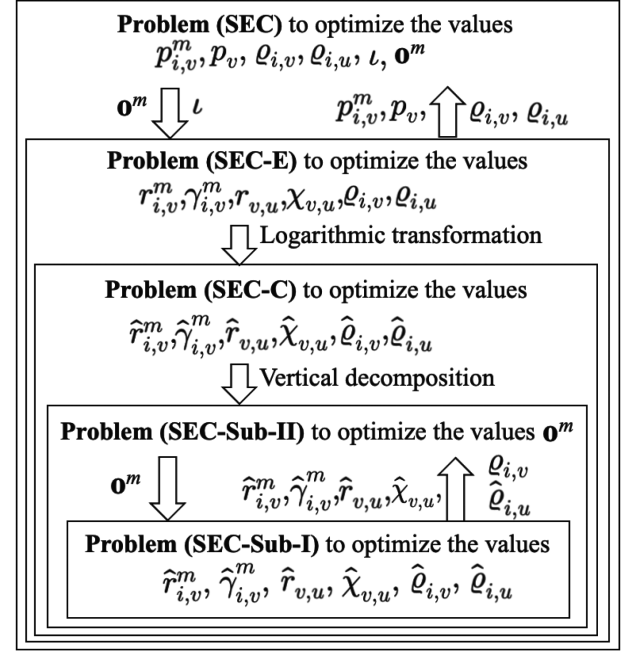$\hat{r}_{i,v}^m \geq 0, \hat{\gamma}_{i,v}^m \geq 0, \hat{r}_{v,u} \geq 0, \hat{\chi}_{v,u} \geq 0,$

Fig. 2. Decomposition process for solving Problem (SEC).

$$\hat{\varrho}_{i,v} \geq 0, \hat{\varrho}_{i,u} \geq 0, \forall i \in \mathcal{I},$$

variables : $\hat{r}_{i,v}^m, \hat{\gamma}_{i,v}^m, \hat{r}_{v,u}, \hat{\chi}_{v,u}, \hat{\varrho}_{i,v}, \hat{\varrho}_{i,u}, \forall i \in \mathcal{I}.$

- (Sub-II) for SIC ordering optimization. After determining the resource allocation strategy, we can further minimize the energy consumption by optimizing $\mathbf{o}^m$, which results in the following problem

(SEC-Sub-II) : $\min \hat{E}^{\text{tot}}$

variables : $\mathbf{o}^m$.

B. Proposed Algorithm for Solving Problem (SEC-Sub-I)

Through a series of decomposition, we have obtained the convex form for Problem (SEC-Sub-I) under the given decoding order $\mathbf{o}^m$. Therefore, we can derive the resource allocation through the Karush-Kuhn-Tucker (KKT) conditions. Let $\theta \geq 0$, $\rho \geq 0$, $\vartheta_i \geq 0$, $\varpi \geq 0$, $\mu_i \geq 0$, $\zeta \geq 0$, $\sigma_i \geq 0$ denote the Lagrangian multipliers corresponding to constraints (41), (42), (43), (44), (45), (46), (47), respectively. The Lagrangian function can be expressed in (48) shown at the bottom of the next page, where $\hat{\mathbf{r}}, \hat{\boldsymbol{\gamma}}, \hat{\boldsymbol{\varrho}}_v, \hat{\boldsymbol{\varrho}}_u, \boldsymbol{\vartheta}, \boldsymbol{\mu}, \boldsymbol{\sigma}$ are the vectors corresponding to $\hat{r}_{i,v}^m, \hat{\gamma}_{i,v}^m, \hat{\varrho}_{i,v}, \hat{\varrho}_{i,u}, \vartheta_i, \mu_i, \sigma_i$, respectively.

We use $\hat{r}_{i,v}^{m,*}, \hat{\gamma}_{i,v}^{m,*}, \hat{r}_{v,u}^*, \hat{\chi}_{v,u}^*, \hat{\varrho}_{i,v}^*, \hat{\varrho}_{i,u}^*$ to denote the optimal solutions of Problem (SEC-Sub-I). It can be obtained by

$$\hat{E}^{\text{tot}} = \log\left\{\sum_{i=1}^{I}\left[\begin{array}{l} \frac{s_i N_v}{g_{i,v}^m}e^{\hat{\gamma}_{i,v}^m - \hat{r}_{i,v}^m}\prod_{j\in\mathcal{I},\mathbf{o}^m(j)<\mathbf{o}^m(i)}\left(1 + e^{\hat{\gamma}_{j,v}^m}\right) + \frac{Q_i N_u}{h_{v,u}}e^{\hat{\chi}_{v,u} - \hat{r}_{v,u}}\left(\dfrac{\omega_2}{e^{\frac{\varphi^{\min}-\omega_4}{\omega_1}}-\omega_3}\right) \\ + \epsilon\left(B_i e^{2\hat{\varrho}_{i,v}} + D_i e^{2\hat{\varrho}_{i,u}}\right)\left(\dfrac{\omega_2}{e^{\frac{\varphi^{\min}-\omega_4}{\omega_1}}-\omega_3}\right)^2 \end{array}\right]\right\}. \tag{40}$$

minimizing the Lagrangian function in (48) and maximizing the Lagrangian dual function. The optimal solutions satisfy the following conditions

$$
\begin{cases}
\frac{\partial \mathcal{L}(\mathbf{o}^m, \hat{r}_{i,v}^m, \bullet)}{\partial \hat{r}_{i,v}^m}\Big|_{\hat{r}_{i,v}^m = \hat{r}_{i,v}^{m,*}} = 0, \forall i \in \mathcal{I}, \\
\frac{\partial \mathcal{L}(\mathbf{o}^m, \hat{\gamma}_{i,v}^m, \bullet)}{\partial \hat{\gamma}_{i,v}^m}\Big|_{\hat{\gamma}_{i,v}^m = \hat{\gamma}_{i,v}^{m,*}} = 0, \forall i \in \mathcal{I}, \\
\frac{\partial \mathcal{L}(\mathbf{o}^m, \hat{r}_{v,u}, \bullet)}{\partial \hat{r}_{v,u}}\Big|_{\hat{r}_{v,u} = \hat{r}_{v,u}^*} = 0, \\
\frac{\partial \mathcal{L}(\mathbf{o}^m, \hat{\chi}_{v,u}, \bullet)}{\partial \hat{\chi}_{v,u}}\Big|_{\hat{\chi}_{v,u} = \hat{\chi}_{v,u}^*} = 0, \\
\frac{\partial \mathcal{L}(\mathbf{o}^m, \hat{\varrho}_{i,v}, \bullet)}{\partial \hat{\varrho}_{i,v}}\Big|_{\hat{\varrho}_{i,v} = \hat{\varrho}_{i,v}^*} = 0, \forall i \in \mathcal{I}, \\
\frac{\partial \mathcal{L}(\mathbf{o}^m, \hat{\varrho}_{i,u}, \bullet)}{\partial \hat{\varrho}_{i,u}}\Big|_{\hat{\varrho}_{i,u} = \hat{\varrho}_{i,u}^*} = 0, \forall i \in \mathcal{I},
\end{cases} \tag{49}
$$

Then, the Lagrangian dual function of (48) can be formulated as

$$
\mathcal{G}(\mathbf{o}^m, \theta, \rho, \boldsymbol{\vartheta}, \varpi, \boldsymbol{\mu}, \zeta, \boldsymbol{\sigma}) =
$$
$$
\min_{\substack{\hat{\boldsymbol{r}}, \hat{\boldsymbol{\gamma}}, \hat{r}_{v,u}, \\ \hat{\chi}_{v,u}, \hat{\boldsymbol{\varrho}}_{\boldsymbol{v}}, \hat{\boldsymbol{\varrho}}_{\boldsymbol{u}}}} \mathcal{L}(\mathbf{o}^m, \hat{\boldsymbol{r}}, \hat{\boldsymbol{\gamma}}, \hat{r}_{v,u}, \hat{\chi}_{v,u}, \hat{\boldsymbol{\varrho}}_{\boldsymbol{v}}, \hat{\boldsymbol{\varrho}}_{\boldsymbol{u}}, \theta, \rho, \boldsymbol{\vartheta}, \varpi, \boldsymbol{\mu}, \zeta, \boldsymbol{\sigma}), \tag{50}
$$

and

(SEC-Sub-I-Dual) : $\max \mathcal{G}(\mathbf{o}^m, \theta, \rho, \boldsymbol{\vartheta}, \varpi, \boldsymbol{\mu}, \zeta, \boldsymbol{\sigma})$

subject to : $\theta \geq 0, \rho \geq 0, \vartheta_i \geq 0, \varpi \geq 0, \mu_i \geq 0,$

$\zeta \geq 0, \sigma_i \geq 0, \forall i \in \mathcal{I},$

variables : $\theta, \rho, \vartheta_i, \varpi, \mu_i, \zeta, \sigma_i, \forall i \in \mathcal{I}.$

The gradient descent approach is utilized to solve the transformed Problem (SEC-Sub-I-Dual). Specifically, we first obtain a descent direction of the optimization variables in (50). Then, the optimization variables in (50) are updated. After that, we update the Lagrangian multipliers in Problem (SEC-Sub-I-Dual) via the subgradient approach.

To determine a descent direction, we first find the initial feasible solutions $\hat{\boldsymbol{r}}^{(0)}, \hat{\boldsymbol{\gamma}}^{(0)}, \hat{r}_{v,u}^{(0)}, \hat{\chi}_{v,u}^{(0)}, \hat{\boldsymbol{\varrho}}_{\boldsymbol{v}}^{(0)}, \hat{\boldsymbol{\varrho}}_{\boldsymbol{u}}^{(0)}$ regarding (50). For the sake of expression, the objective function in Problem (SEC-C) is rewritten as $\hat{E}^{\text{tot}} = \log \kappa(\hat{\boldsymbol{r}}, \hat{\boldsymbol{\gamma}}, \hat{r}_{v,u}, \hat{\chi}_{v,u}, \hat{\boldsymbol{\varrho}}_{\boldsymbol{v}}, \hat{\boldsymbol{\varrho}}_{\boldsymbol{u}}) = \log \kappa(\bullet)$. The first derivative of Lagrangian function in (48)

regarding variables of $\hat{r}_{i,v}^m, \hat{\gamma}_{i,v}^m, \hat{r}_{v,u}, \hat{\chi}_{v,u}, \hat{\varrho}_{i,v}, \hat{\varrho}_{i,u}$ can be separately denoted as

$$
\frac{\partial \mathcal{L}(\mathbf{o}^m, \hat{r}_{i,v}^m, \bullet)}{\partial \hat{r}_{i,v}^m} =
$$
$$
-\frac{s_i N_v}{\kappa(\bullet) g_{i,v}^m} e^{\hat{\gamma}_{i,v}^m - \hat{r}_{i,v}^m} \prod_{j \in \mathcal{I}, \mathbf{o}^m(j) < \mathbf{o}^m(i)} \left(1 + e^{\hat{\gamma}_{j,v}^m}\right)
$$
$$
+ \mu_i - \frac{\sigma_i s_i e^{-\hat{r}_{i,v}^m}}{\left[\begin{array}{c} s_i e^{-\hat{r}_{i,v}^m} + Q_i e^{-\hat{r}_{v,u}} \left(\dfrac{\omega_2}{e^{\frac{\varphi^{\min} - \omega_4}{\omega_1}} - \omega_3}\right) \\ + \left(\dfrac{\omega_2}{e^{\frac{\varphi^{\min} - \omega_4}{\omega_1}} - \omega_3}\right)^2 \left(B_i e^{-\hat{\varrho}_{i,v}} + D_i e^{-\hat{\varrho}_{i,u}}\right) \end{array}\right]}. \tag{51}
$$

$$
\frac{\partial \mathcal{L}(\mathbf{o}^m, \hat{\gamma}_{i,v}^m, \bullet)}{\partial \hat{\gamma}_{i,v}^m} = \frac{N_v}{\kappa(\bullet)}
$$
$$
\times \left[\begin{array}{c} \frac{s_i}{g_{i,v}^m} e^{\hat{\gamma}_{i,v}^m - \hat{r}_{i,v}^m} \prod_{j \in \mathcal{I}, \mathbf{o}^m(j) < \mathbf{o}^m(i)} \left(1 + e^{\hat{\gamma}_{j,v}^m}\right) \\ + \sum_{k=1}^{i-1} \left(\frac{s_k}{g_{k,v}^m} e^{\hat{\gamma}_{k,v}^m - \hat{r}_{k,v}^m} \prod_{n=k+1}^{I} \left(1 + e^{\hat{\gamma}_{n,v}^m}\right)\right) \end{array}\right]
$$
$$
- \frac{\mu_i e^{\hat{\gamma}_{i,v}^m}}{\ln 2 \left(1 + e^{\hat{\gamma}_{i,v}^m}\right) \log_2 \left(1 + e^{\hat{\gamma}_{i,v}^m}\right)} + \vartheta_i + \frac{e^{\hat{\gamma}_{i,v}^m}}{1 + e^{\hat{\gamma}_{i,v}^m}} \sum_{k=1}^{i-1} \vartheta_i. \tag{52}
$$

$$
\frac{\partial \mathcal{L}(\mathbf{o}^m, \hat{r}_{v,u}, \bullet)}{\partial \hat{r}_{v,u}} = -\frac{N_u e^{\hat{\chi}_{v,u} - \hat{r}_{v,u}}}{h_{v,u} \kappa(\bullet)} \left(\frac{\omega_2}{e^{\frac{\varphi^{\min} - \omega_4}{\omega_1}} - \omega_3}\right) \sum_{i=1}^{I} Q_i
$$
$$
+ \zeta - \sum_{i=1}^{I} \frac{\sigma_i Q_i e^{-\hat{r}_{v,u}} \left(\dfrac{\omega_2}{e^{\frac{\varphi^{\min} - \omega_4}{\omega_1}} - \omega_3}\right)}{\left[\begin{array}{c} s_i e^{-\hat{r}_{i,v}^m} + Q_i e^{-\hat{r}_{v,u}} \left(\dfrac{\omega_2}{e^{\frac{\varphi^{\min} - \omega_4}{\omega_1}} - \omega_3}\right) + \\ \left(\dfrac{\omega_2}{e^{\frac{\varphi^{\min} - \omega_4}{\omega_1}} - \omega_3}\right)^2 \left(B_i e^{-\hat{\varrho}_{i,v}} + D_i e^{-\hat{\varrho}_{i,u}}\right) \end{array}\right]}. \tag{53}
$$

$$
\mathcal{L}(\mathbf{o}^m, \hat{\boldsymbol{r}}, \hat{\boldsymbol{\gamma}}, \hat{r}_{v,u}, \hat{\chi}_{v,u}, \hat{\boldsymbol{\varrho}}_{\boldsymbol{v}}, \hat{\boldsymbol{\varrho}}_{\boldsymbol{u}}, \theta, \rho, \boldsymbol{\vartheta}, \varpi, \boldsymbol{\mu}, \zeta, \boldsymbol{\sigma}) =
$$
$$
\log\left\{\sum_{i=1}^{I}\left[\begin{array}{c}\frac{s_i N_v}{g_{i,v}^m} e^{\hat{\gamma}_{i,v}^m - \hat{r}_{i,v}^m} \prod_{j \in \mathcal{I}, \mathbf{o}^m(j) < \mathbf{o}^m(i)}\left(1 + e^{\hat{\gamma}_{j,v}^m}\right) + \left(\frac{Q_i N_u}{h_{v,u}} e^{\hat{\chi}_{v,u} - \hat{r}_{v,u}}\right) \\ \times \left(\frac{\omega_2}{e^{\frac{\varphi^{\min} - \omega_4}{\omega_1}} - \omega_3}\right) + \epsilon\left(B_i e^{2\hat{\varrho}_{i,v}} + D_i e^{2\hat{\varrho}_{i,u}}\right)\left(\frac{\omega_2}{e^{\frac{\varphi^{\min} - \omega_4}{\omega_1}} - \omega_3}\right)^2\end{array}\right]\right\} + \theta\left[\log\left(\sum_{i=1}^{I} e^{\hat{\varrho}_{i,v}}\right) - \log \varrho_v^{\max}\right]
$$
$$
+ \rho\left[\log\left(\sum_{i=1}^{I} e^{\hat{\varrho}_{i,u}}\right) - \log \varrho_u^{\max}\right] + \sum_{i=1}^{I} \vartheta_i\left[\hat{\gamma}_{i,v}^m + \sum_{j \in \mathcal{I}, \mathbf{o}^m(j) < \mathbf{o}^m(i)} \log\left(1 + e^{\hat{\gamma}_{j,v}^m}\right) - \log\frac{P^{\max} g_{i,v}^m}{N_v}\right]
$$
$$
+ \varpi\left(\hat{\chi}_{v,u} - \log\frac{P^{\max} h_{v,u}}{N_u}\right) + \sum_{i=1}^{I} \mu_i\left[\hat{r}_{i,v}^m - \log\left(W\log_2\left(1 + e^{\hat{\gamma}_{i,v}^m}\right)\right)\right] + \zeta\left(\hat{r}_{v,u} - \log\left(\hat{W}\log_2\left(1 + e^{\hat{\chi}_{v,u}}\right)\right)\right)
$$
$$
+ \sum_{i=1}^{I} \sigma_i\left\{\log\left[s_i e^{-\hat{r}_{i,v}^m} + Q_i e^{-\hat{r}_{v,u}}\left(\frac{\omega_2}{e^{\frac{\varphi^{\min} - \omega_4}{\omega_1}} - \omega_3}\right) + \left(\frac{\omega_2}{e^{\frac{\varphi^{\min} - \omega_4}{\omega_1}} - \omega_3}\right)^2\left(B_i e^{-\hat{\varrho}_{i,v}} + D_i e^{-\hat{\varrho}_{i,u}}\right)\right] - \log T^{\max}\right\}. \tag{48}
$$

$$\frac{\partial \mathcal{L}\left(\mathbf{o}^m, \hat{\chi}_{v,u}, \bullet\right)}{\partial \hat{\chi}_{v,u}} = \frac{N_u e^{\hat{\chi}_{v,u} - \hat{r}_{v,u}}}{h_{v,u} \kappa\left(\bullet\right)} \left(\frac{\omega_2}{e^{\frac{\varphi^{\min} - \omega_4}{\omega_1}} - \omega_3}\right) \sum_{i=1}^{I} Q_i$$

$$+ \varpi - \frac{\zeta e^{\hat{\chi}_{v,u}}}{\ln 2 \left(1 + e^{\hat{\chi}_{v,u}}\right) \hat{W} \log_2\left(1 + e^{\hat{\chi}_{v,u}}\right)}. \qquad (54)$$

$$\frac{\partial \mathcal{L}\left(\mathbf{o}^m, \hat{\varrho}_{i,v}, \bullet\right)}{\partial \hat{\varrho}_{i,v}} = \frac{2\epsilon B_i e^{2\hat{\varrho}_{i,v}}}{\kappa\left(\bullet\right)} \left(\frac{\omega_2}{e^{\frac{\varphi^{\min} - \omega_4}{\omega_1}} - \omega_3}\right)^2 +$$

$$\frac{\theta e^{\hat{\varrho}_{i,v}}}{\sum\limits_{i=1}^{I} e^{\hat{\varrho}_{i,v}}} - \frac{\sigma_i B_i e^{-\hat{\varrho}_{i,v}} \left(\frac{\omega_2}{e^{\frac{\varphi^{\min} - \omega_4}{\omega_1}} - \omega_3}\right)^2}{\left[\begin{array}{c} s_i e^{-\hat{r}_{i,v}^m} + Q_i e^{-\hat{r}_{i,u}} \left(\frac{\omega_2}{e^{\frac{\varphi^{\min} - \omega_4}{\omega_1}} - \omega_3}\right) + \\ \left(\frac{\omega_2}{e^{\frac{\varphi^{\min} - \omega_4}{\omega_1}} - \omega_3}\right)^2 \left(B_i e^{-\hat{\varrho}_{i,v}} + D_i e^{-\hat{\varrho}_{i,u}}\right) \end{array}\right]}. \qquad (55)$$

$$\frac{\partial \mathcal{L}\left(\mathbf{o}^m, \hat{\varrho}_{i,u}, \bullet\right)}{\partial \hat{\varrho}_{i,u}} = \frac{2\epsilon D_i e^{2\hat{\varrho}_{i,u}}}{\kappa\left(\bullet\right)} \left(\frac{\omega_2}{e^{\frac{\varphi^{\min} - \omega_4}{\omega_1}} - \omega_3}\right)^2 +$$

$$\frac{\theta e^{\hat{\varrho}_{i,u}}}{\sum\limits_{i=1}^{I} e^{\hat{\varrho}_{i,u}}} - \frac{\sigma_i D_i e^{-\hat{\varrho}_{i,u}} \left(\frac{\omega_2}{e^{\frac{\varphi^{\min} - \omega_4}{\omega_1}} - \omega_3}\right)^2}{\left[\begin{array}{c} s_i e^{-\hat{r}_{i,v}^m} + Q_i e^{-\hat{r}_{i,u}} \left(\frac{\omega_2}{e^{\frac{\varphi^{\min} - \omega_4}{\omega_1}} - \omega_3}\right) + \\ \left(\frac{\omega_2}{e^{\frac{\varphi^{\min} - \omega_4}{\omega_1}} - \omega_3}\right)^2 \left(B_i e^{-\hat{\varrho}_{i,v}} + D_i e^{-\hat{\varrho}_{i,u}}\right) \end{array}\right]}. \qquad (56)$$

Then, we use $\hat{r}^{(\delta-1)}, \hat{\gamma}^{(\delta-1)}, \hat{r}_{v,u}^{(\delta-1)}, \hat{\chi}_{v,u}^{(\delta-1)}, \hat{\varrho}_{v}^{(\delta-1)}, \hat{\varrho}_{u}^{(\delta-1)}$ to denote the updated variables of Problem (SEC-Sub-I-Dual) at the $(\delta-1)$-th iteration, and use $\theta^{(\delta-1)}, \rho^{(\delta-1)}, \vartheta^{(\delta-1)}, \varpi^{(\delta-1)}$, $\mu^{(\delta-1)}, \zeta^{(\delta-1)}, \sigma^{(\delta-1)}$ to represent the Lagrangian multiplier variables at the $(\delta-1)$-th iteration. The descent direction of the optimization variables in Problem (SEC-Sub-I-Dual) at the δ-th iteration can be expressed as follows

$$\left\{\begin{array}{l} \Lambda_{\hat{r}_{i,v}^m}^{(\delta)} = -\frac{\partial \mathcal{L}\left(\mathbf{o}^m, \hat{r}_{i,v}^m, \bullet\right)}{\partial \hat{r}_{i,v}^m} \Big|_{\substack{\hat{r}^{(\delta-1)}, \hat{\gamma}^{(\delta-1)}, \hat{r}_{v,u}^{(\delta-1)}, \hat{\chi}_{v,u}^{(\delta-1)}, \\ \hat{\varrho}_{v}^{(\delta-1)}, \hat{\varrho}_{u}^{(\delta-1)}, \mu^{(\delta-1)}, \sigma^{(\delta-1)}}} \\[6pt] \Lambda_{\hat{\gamma}_{i,v}^m}^{(\delta)} = -\frac{\partial \mathcal{L}\left(\mathbf{o}^m, \hat{\gamma}_{i,v}^m, \bullet\right)}{\partial \hat{\gamma}_{i,v}^m} \Big|_{\substack{\hat{r}^{(\delta-1)}, \hat{\gamma}^{(\delta-1)}, \hat{r}_{v,u}^{(\delta-1)}, \hat{\chi}_{v,u}^{(\delta-1)}, \\ \hat{\varrho}_{v}^{(\delta-1)}, \hat{\varrho}_{u}^{(\delta-1)}, \vartheta^{(\delta-1)}, \mu^{(\delta-1)}}} \\[6pt] \Lambda_{\hat{r}_{v,u}}^{(\delta)} = -\frac{\partial \mathcal{L}\left(\mathbf{o}^m, \hat{r}_{v,u}, \bullet\right)}{\partial \hat{r}_{v,u}} \Big|_{\substack{\hat{r}^{(\delta-1)}, \hat{\gamma}^{(\delta-1)}, \hat{r}_{v,u}^{(\delta-1)}, \hat{\chi}_{v,u}^{(\delta-1)}, \\ \hat{\varrho}_{v}^{(\delta-1)}, \hat{\varrho}_{u}^{(\delta-1)}, \zeta^{(\delta-1)}, \sigma^{(\delta-1)}}} \\[6pt] \Lambda_{\hat{\chi}_{v,u}}^{(\delta)} = -\frac{\partial \mathcal{L}\left(\mathbf{o}^m, \hat{\chi}_{v,u}, \bullet\right)}{\partial \hat{\chi}_{v,u}} \Big|_{\substack{\hat{r}^{(\delta-1)}, \hat{\gamma}^{(\delta-1)}, \hat{r}_{v,u}^{(\delta-1)}, \hat{\chi}_{v,u}^{(\delta-1)}, \\ \hat{\varrho}_{v}^{(\delta-1)}, \hat{\varrho}_{u}^{(\delta-1)}, \varpi^{(\delta-1)}, \zeta^{(\delta-1)}}} \\[6pt] \Lambda_{\hat{\varrho}_{i,v}}^{(\delta)} = -\frac{\partial \mathcal{L}\left(\mathbf{o}^m, \hat{\varrho}_{i,v}, \bullet\right)}{\partial \hat{\varrho}_{i,v}} \Big|_{\substack{\hat{r}^{(\delta-1)}, \hat{\gamma}^{(\delta-1)}, \hat{r}_{v,u}^{(\delta-1)}, \hat{\chi}_{v,u}^{(\delta-1)}, \\ \hat{\varrho}_{v}^{(\delta-1)}, \hat{\varrho}_{u}^{(\delta-1)}, \theta^{(\delta-1)}, \sigma^{(\delta-1)}}} \\[6pt] \Lambda_{\hat{\varrho}_{i,u}}^{(\delta)} = -\frac{\partial \mathcal{L}\left(\mathbf{o}^m, \hat{\varrho}_{i,u}, \bullet\right)}{\partial \hat{\varrho}_{i,u}} \Big|_{\substack{\hat{r}^{(\delta-1)}, \hat{\gamma}^{(\delta-1)}, \hat{r}_{v,u}^{(\delta-1)}, \hat{\chi}_{v,u}^{(\delta-1)}, \\ \hat{\varrho}_{v}^{(\delta-1)}, \hat{\varrho}_{u}^{(\delta-1)}, \rho^{(\delta-1)}, \sigma^{(\delta-1)}}} \end{array}\right. \qquad (57)$$

Next, we use η to denote the step size when updating the optimization variables. The optimization variables $\hat{r}^{(\delta)}, \hat{\gamma}^{(\delta)}$, $\hat{r}_{v,u}^{(\delta)}, \hat{\chi}_{v,u}^{(\delta)}, \hat{\varrho}_{v}^{(\delta)}, \hat{\varrho}_{u}^{(\delta)}$ are updated at the δ-th iteration as follows

$$\left\{\begin{array}{l} \hat{r}_{i,v}^{m(\delta)} = \hat{r}_{i,v}^{m(\delta-1)} + \eta^{(\delta)} \Lambda_{\hat{r}_{i,v}^m}^{(\delta)} \\ \hat{\gamma}_{i,v}^{m(\delta)} = \hat{\gamma}_{i,v}^{m(\delta-1)} + \eta^{(\delta)} \Lambda_{\hat{\gamma}_{i,v}^m}^{(\delta)} \\ \hat{r}_{v,u}^{(\delta)} = \hat{r}_{v,u}^{(\delta-1)} + \eta^{(\delta)} \Lambda_{\hat{r}_{v,u}}^{(\delta)} \\ \hat{\chi}_{v,u}^{(\delta)} = \hat{\chi}_{v,u}^{(\delta-1)} + \eta^{(\delta)} \Lambda_{\hat{\chi}_{v,u}}^{(\delta)} \\ \hat{\varrho}_{i,v}^{(\delta)} = \hat{\varrho}_{i,v}^{(\delta-1)} + \eta^{(\delta)} \Lambda_{\hat{\varrho}_{i,v}}^{(\delta)} \\ \hat{\varrho}_{i,u}^{(\delta)} = \hat{\varrho}_{i,u}^{(\delta-1)} + \eta^{(\delta)} \Lambda_{\hat{\varrho}_{i,u}}^{(\delta)} \end{array}\right. \qquad (58)$$

Finally, we use ς to denote the step size when updating the multipliers. The Lagrangian multiplier variables $\theta^{(\delta)}, \rho^{(\delta)}, \vartheta^{(\delta)}$, $\varpi^{(\delta)}, \mu^{(\delta)}, \zeta^{(\delta)}, \sigma^{(\delta)}$ are updated based on subgradient method at the δ-th iteration as follows

$$\theta^{(\delta)} =$$
$$\left\lfloor \theta^{(\delta-1)} + \varsigma^{(\delta)} \left(\log\left(\sum_{i=1}^{I} e^{\hat{\varrho}_{i,v}^{(\delta)}}\right) - \log \varrho_v^{\max}\right), 0 \right\rfloor. \qquad (59)$$

$$\rho^{(\delta)} =$$
$$\left\lfloor \rho^{(\delta-1)} + \varsigma^{(\delta)} \left(\log\left(\sum_{i=1}^{I} e^{\hat{\varrho}_{i,u}^{(\delta)}}\right) - \log \varrho_u^{\max}\right), 0 \right\rfloor. \qquad (60)$$

$$\vartheta_i^{(\delta)} =$$
$$\left\lfloor \vartheta_i^{(\delta-1)} + \varsigma^{(\delta)} \times \left(\begin{array}{c} \hat{\gamma}_{i,v}^{m(\delta)} - \log \frac{P^{\max} g_{i,v}^m}{N_v} \\ + \sum_{j \in \mathcal{I}, \mathbf{o}^m(j) < \mathbf{o}^m(i)} \log\left(1 + e^{\hat{\gamma}_{j,v}^{m(\delta)}}\right) \end{array}\right), 0 \right\rfloor, \forall i \in \mathcal{I}. \qquad (61)$$

$$\varpi^{(\delta)} = \left\lfloor \varpi^{(\delta-1)} + \varsigma^{(\delta)} \left(\hat{\chi}_{v,u}^{(\delta)} - \log \frac{P^{\max} h_{i,u}}{N_u}\right), 0 \right\rfloor. \qquad (62)$$

$$\mu_i^{(\delta)} =$$
$$\left\lfloor \mu_i^{(\delta-1)} + \varsigma^{(\delta)} \times \left(\hat{r}_{i,v}^{m(\delta)} - \log\left(W \log_2\left(1 + e^{\hat{\gamma}_{i,v}^{m(\delta)}}\right)\right)\right), 0 \right\rfloor, \forall i \in \mathcal{I}. \qquad (63)$$

$$\zeta^{(\delta)} = \left\lfloor \zeta^{(\delta-1)} + \varsigma^{(\delta)} \times \left(\hat{r}_{v,u}^{(\delta)} - \log\left(\hat{W} \log_2\left(1 + e^{\hat{\chi}_{v,u}^{(\delta)}}\right)\right)\right), 0 \right\rfloor. \qquad (64)$$

$$\sigma_i^{(\delta)} = \left\lfloor \sigma_i^{(\delta-1)} + \varsigma^{(\delta)} \times \left(\log\left[\begin{array}{c} s_i e^{-\hat{r}_{i,v}^{m(\delta)}} \\ + Q_i e^{-\hat{r}_{v,u}^{(\delta)}} \left(\frac{\omega_2}{e^{\frac{\varphi^{\min} - \omega_4}{\omega_1}} - \omega_3}\right) \\ + \left(\frac{\omega_2}{e^{\frac{\varphi^{\min} - \omega_4}{\omega_1}} - \omega_3}\right)^2 \\ \times \left(B_i e^{-\hat{\varrho}_{i,v}^{(\delta)}} + D_i e^{-\hat{\varrho}_{i,u}^{(\delta)}}\right) \end{array}\right] - \log T^{\max}\right), 0 \right\rfloor,$$
$$\forall i \in \mathcal{I}. \qquad (65)$$

Algorithm 1: Resource Allocation Algorithm for Solving Problem (SEC-Sub-I-Dual).

1:   **Input:** The computation error ∇, the updating step size ς and η, the fixed decoding order $\mathbf{o}^m$, the optimal scaling factor ι^*;

2:   **Initialization:** set $\delta = 1$, set ∇ as a small value, set ς and η as the small values. Find the feasible solutions $\hat{r}^{(0)}, \hat{\gamma}^{(0)}, \hat{r}_{v,u}^{(0)}, \hat{\chi}_{v,u}^{(0)}, \hat{\varrho}_v^{(0)}, \hat{\varrho}_u^{(0)}$ for Problem (SEC-Sub-I-Dual), initialize the feasible Lagrangian multipliers $\theta^{(0)}, \rho^{(0)}, \vartheta^{(0)}, \varpi^{(0)}, \mu^{(0)}, \zeta^{(0)}, \sigma^{(0)}$. ;

3:   **while** $\{\Lambda_{\hat{r}_{i,v}^m}^{(\delta)}, \Lambda_{\hat{\gamma}_{i,v}^m}^{(\delta)}, \Lambda_{\hat{r}_{v,u}}^{(\delta)}, \Lambda_{\hat{\chi}_{v,u}}^{(\delta)}, \Lambda_{\hat{\varrho}_{i,v}}^{(\delta)}, \Lambda_{\hat{\varrho}_{i,u}}^{(\delta)}\} \leq \nabla$ **do**

4:      Compute the descent direction of the feasible solutions by (57);

5:      Compute the optimization values at the current iteration by (58);

6:      Update the Lagrangian multipliers from (59) to (65);

7:      Update $\delta \leftarrow \delta + 1$;

8:   **end**

9:   **Output:** The optimal solutions $\hat{r}^*, \hat{\gamma}^*, \hat{r}_{v,u}^*, \hat{\chi}_{v,u}^*, \hat{\varrho}_v^*, \hat{\varrho}_u^*$, denoted as $\hat{r}^{(\delta-1)}, \hat{\gamma}^{(\delta-1)}, \hat{r}_{v,u}^{(\delta-1)}, \hat{\chi}_{v,u}^{(\delta-1)}, \hat{\varrho}_v^{(\delta-1)}, \hat{\varrho}_u^{(\delta-1)}$;

In (59), (60), (61), (62), (63), (64), (65), $\lfloor \times, 0 \rfloor = \max\{\times, 0\}$. Let ∇ denote the computation error, which is a small positive constant. The optimization variables and multiplier variables are repeated based on the above procedure until the computation error is satisfied, i.e., $\{\Lambda_{\hat{r}_{i,v}^m}^{(\delta)}, \Lambda_{\hat{\gamma}_{i,v}^m}^{(\delta)}, \Lambda_{\hat{r}_{v,u}}^{(\delta)}, \Lambda_{\hat{\chi}_{v,u}}^{(\delta)}, \Lambda_{\hat{\varrho}_{i,v}}^{(\delta)}, \Lambda_{\hat{\varrho}_{i,u}}^{(\delta)}\} \leq \nabla, \forall i \in \mathcal{I}$. Algorithm 1 shows the resource allocation algorithm for solving Problem (SEC-Sub-I-Dual). The details are illustrated as follows.

- *Step 1-Step 2:* We first initialize the computation error ∇ and the step size ς and η. Then, we determine a decoding order $\mathbf{o}^m$, and find the feasible solutions and Lagrangian multipliers.

- *Step 3-Step 8:* We calculate the descent direction of the solutions and the optimization values. Then, we update the Lagrangian multipliers until the computation error ∇ is satisfied.

- *Step 9:* We finally output the optimal resource allocation solutions of Problem (SEC-Sub-I-Dual) as $\hat{r}^{(\delta-1)}, \hat{\gamma}^{(\delta-1)}, \hat{r}_{v,u}^{(\delta-1)}, \hat{\chi}_{v,u}^{(\delta-1)}, \hat{\varrho}_v^{(\delta-1)}, \hat{\varrho}_u^{(\delta-1)}$.

C. Proposed Algorithm for Solving Problem (SEC-Sub-II)

Notice that different decoding orders can yield different throughput of UAVs (i.e., $r_{i,v}^m$). In this subsection, we aim to determine the SIC ordering to further minimize the system consumption. It is impractical to enumerate for obtaining the optimal SIC ordering. In order to reduce the complexity for seeking the SIC ordering, we aim to design a sub-optimal SIC ordering algorithm via Tabu searching algorithm [50], which can find the sub-optimal SIC ordering via seeking the neighboring

solution that is excluded in the Tabu list. This avoids re-searching the promising SIC ordering during the iterations.

Before conducting the Tabu searching algorithm, we first find an initial feasible solution (i.e., SIC ordering $\mathbf{o}^{(0)}$). Let Θ be the Tabu list, and the initial value is set as $\Theta^{(0)} \leftarrow \emptyset$. We consider a decoding order as $\mathbf{o}^{(\ell-1)} = o_1^{(\ell-1)} \rightarrow \cdots \rightarrow o_i^{(\ell-1)} \rightarrow o_j^{(\ell-1)} \cdots \rightarrow o_I^{(\ell-1)}$ at the $(\ell-1)$th iteration.

Then, at the ℓ-th iteration, we generate the neighboring solution $\mathbf{S}^{(m)}$ through changing the SIC ordering of any two UAVs in $\mathbf{o}^{(\ell-1)}$. The neighboring solution is denoted as $\mathbf{S}^{(m)} = \langle \hat{\mathbf{o}}^{(\ell-1)} | \mathcal{F}(\hat{\mathbf{o}}^{(\ell-1)}) \rangle_{i,j \in \mathcal{I}, i \neq j}$, where $\hat{\mathbf{o}}^{(\ell-1)} = o_1^{(\ell-1)} \rightarrow \cdots \rightarrow o_j^{(\ell-1)} \rightarrow o_i^{(\ell-1)} \cdots \rightarrow o_I^{(\ell-1)}$. $\mathcal{F}(\hat{\mathbf{o}}^{(\ell-1)})$ denotes the objective function in Problem (SEC-Sub-II), and the value of $\mathcal{F}(\hat{\mathbf{o}}^{(\ell-1)})$ can be obtained by the proposed Algorithm 1 with the SIC ordering $\hat{\mathbf{o}}^{(\ell-1)}$. Here, if the SIC ordering $\hat{\mathbf{o}}^{(\ell-1)}$ is infeasible, we set the value of $\mathcal{F}(\hat{\mathbf{o}}^{(\ell-1)})$ to be ∞.

Next, at the ℓ-th iteration, we choose the best solution $\mathbf{o}^{(\ell)}$ from the neighboring solution that is eliminated in the Tabu list $\mathbf{S}^{(\ell)} \backslash \Theta^{(\ell-1)}$, which can be expressed as

$$\mathbf{o}^{(\ell)} = \underset{\langle \mathbf{o}^{(\ell)} | \mathcal{F}(\mathbf{o}^{(\ell)}) \rangle \in \mathbf{S}^{(\ell)} \backslash \Theta^{(\ell-1)}}{\arg\min} \mathcal{F}\left(\mathbf{o}^{(\ell)}\right),$$
$$i, j \in \mathcal{I}, i \neq j. \quad (66)$$

Therefore, the current best solution (i.e., SIC ordering $\mathbf{o}^{(\ell)*}$) is derived as

$$\mathbf{o}^{(\ell)*} = \begin{cases} \mathbf{o}^{(\ell-1)*} & \text{if } \mathcal{F}\left(\mathbf{o}^{(\ell-1)*}\right) \leq \mathcal{F}\left(\mathbf{o}^{(\ell)}\right) \\ \mathbf{o}^{(\ell)} & \text{otherwise} \end{cases},$$
$$i, j \in \mathcal{I}, i \neq j. \quad (67)$$

Finally, we stop the Tabu searching if $\mathbf{o}^{(\ell)}$ is infeasible, and we can derive the sub-optimal SIC ordering as $\mathbf{o}^{(\ell)*}$. Otherwise, we need to update the Tabu list $\Theta^{(\ell)}$ that has stored the visited L solutions, denoted as $\Theta^{(\ell)} = \{\langle \mathbf{o}^{(\ell-L+1)} | \mathcal{F}(\mathbf{o}^{(\ell-L+1)}) \rangle, \ldots, \langle \mathbf{o}^{(\ell)} | \mathcal{F}(\mathbf{o}^{(\ell)}) \rangle\}$.

The proposed sub-optimal SIC ordering algorithm is shown in Algorithm 2. We explain the details of Algorithm 2 as follows.

- *Step 1-Step 2:* We first find an initial feasible SIC ordering $\mathbf{o}^{(0)}$ for Problem (SEC-Sub-II), and set the initial Tabu list as $\Theta^{(0)} \leftarrow \emptyset$. Then, we run Algorithm 1 to obtain the resource allocation solutions $\hat{r}^*, \hat{\gamma}^*, \hat{r}_{v,u}^*, \hat{\chi}_{v,u}^*, \hat{\varrho}_v^*, \hat{\varrho}_u^*$.

- *Step 3-Step 13:* We first generate the neighboring solution $\mathbf{S}^{(m)} = \langle \hat{\mathbf{o}}^{(\ell-1)} | \mathcal{F}(\hat{\mathbf{o}}^{(\ell-1)}) \rangle_{i,j \in \mathcal{I}, i \neq j}$ through changing the SIC ordering of any two UAVs in $\mathbf{o}^{(\ell-1)}$. Then, we calculate the objective value of $\mathcal{F}(\hat{\mathbf{o}}^{(\ell-1)})$ by Algorithm 1 with the SIC ordering $\hat{\mathbf{o}}^{(\ell-1)}$, and choose the best solution $\mathbf{o}^{(\ell)}$ from the neighboring solution in the Tabu list $\mathbf{S}^{(\ell)} \backslash \Theta^{(\ell-1)}$ that can minimize the objective value. Next, we record the current best solution $\mathbf{o}^{(\ell)*}$ and repeat the above process.

- *Step 4:* We finally output the sub-optimal SIC ordering of Problem (SEC-Sub-II) as $\mathbf{o}^{(\ell-1)*}$ until $\mathbf{o}^{(\ell)}$ is infeasible.

Algorithm 2: Sub-Optimal SIC Ordering Algorithm for Solving Problem (SEC-Sub-II).

1: **Input:** The resource allocation solutions $\hat{r}^*$, $\hat{\gamma}^*$, $\hat{r}^*_{v,u}$, $\hat{\chi}^*_{v,u}$, $\hat{\varrho}^*_v$, $\hat{\varrho}^*_u$ outputted by Algorithm 1;
2: **Initialization:** Find an initial feasible SIC ordering $\mathbf{o}^{(0)}$, set the initial Tabu list as $\Theta^{(0)} \leftarrow \emptyset$, set $\ell = 1$;
3: **while** $\mathbf{o}^{(\ell)}$ *is infeasible* **do**
4:     Generate the neighboring solution $\mathbf{S}^{(m)}$ through changing the SIC ordering of any two UAVs in $\mathbf{o}^{(\ell-1)}$;
5:     Calculate the objective value $\mathcal{F}(\hat{\mathbf{o}}^{(\ell-1)})$ by the outputted solutions in Algorithm 1 with the SIC ordering $\hat{\mathbf{o}}^{(\ell-1)}$;
6:     **if** $\hat{\mathbf{o}}^{(\ell-1)}$ *is infeasible* **then**
7:         Set $\mathcal{F}(\hat{\mathbf{o}}^{(\ell-1)}) \leftarrow \infty$;
8:     **end**
9:     Choose the best solution $\mathbf{o}^{(\ell)}$ from the neighboring solution $\mathbf{S}^{(\ell)} \setminus \Theta^{(\ell-1)}$ based on (66);
10:    Store the current best solution $\mathbf{o}^{(\ell)*}$ based on (67);
11:    Update the Tabu list $\Theta^{(\ell)}$ as $\Theta^{(\ell)} = \{\langle \mathbf{o}^{(\ell-L+1)} | \mathcal{F}(\mathbf{o}^{(\ell-L+1)})\rangle, \ldots, \langle \mathbf{o}^{(\ell)} | \mathcal{F}(\mathbf{o}^{(\ell)})\rangle\}$;
12:    Update $\ell \leftarrow \ell + 1$;
13: **end**
14: **Output:** The sub-optimal SIC ordering as $\mathbf{o}^{(\ell-1)*}$;

D. Optimality Analysis of Our Proposed Algorithms

In this subsection, we show the optimality analysis for our proposed algorithms. To solve the original formulated Problem (SEC), we first derive the optimal semantic scaling factor ι^* based on Proposition 1. Then, we derive the equivalent Problem (SEC-E) regarding the original problem. Through the logarithmic domain conversion, the equivalent form is transformed into a convex optimization by Proposition 2. By analyzing the characteristic of Problem (SEC-C), we can solve it through alternatively solving two sub-problems, i.e., Problem (SEC-Sub-I) for solving the resource allocation $\hat{r}^m_{i,v}$, $\hat{\gamma}^m_{i,v}$, $\hat{r}_{v,u}$, $\hat{\chi}_{v,u}$, $\hat{\varrho}_{i,v}$, $\hat{\varrho}_{i,u}$; Problem (SEC-Sub-II) for solving the SIC ordering $\mathbf{o}^m$. Regarding Problem (SEC-Sub-I), we obtain the optimal resource allocation solutions $\hat{r}^{m*}_{i,v}, \hat{\gamma}^{m*}_{i,v}, \hat{r}^*_{v,u}, \hat{\chi}^*_{v,u}, \hat{\varrho}^*_{i,v}, \hat{\varrho}^*_{i,u}$ through KKT conditions. In Algorithm 1, we use $\delta^{\max}$ to denote the maximum iterations. The optimization variables and Lagrange multipliers are coupled and updated during each iteration. Therefore, the computational complexity based on KKT conditions for solving Problem (SEC-Sub-I) is $\mathcal{O}(I^2 \log(\delta^{\max}))$. Regarding Problem (SEC-Sub-II), we adopt the Tabu searching approach to obtain the sub-optimal SIC ordering $\mathbf{o}^{m*}$. The maximum number of SIC orderings is $I!$. The computational complexity for solving Problem (SEC-Sub-II) is $\mathcal{O}(LI!)$. The optimization algorithm is based on the product of the solving two sub-problems. To this end, the computational complexity of the optimization Problem (SEC) is $\mathcal{O}(LI^2I!\log(\delta^{\max}))$.

V. PERFORMANCE EVALUATION

This section conducts simulations to validate the performance of the proposed scheme and algorithms. We first introduce the

TABLE III
SIMULATION PARAMETERS

Parameters	Values
α, the channel power gain	10^{-4}
σ, the path loss exponent	2
s_i, the data size required to transmit to the buoy	$[5, 100]$Mb
W, the uplink channel bandwidth	2MHz
$\hat{W}$, the bandwidth for semantic transmission	1MHz
N_v, the additive Gaussian noise at the buoy	-70dBm
N_u, the additive ocean noise at the UDC	-70dBm
B_i, the computation workload for encoding	$[5, 10]$Mb
Q_i, the size of semantic information	$[1, 10]$Kb
D_i, the computing workload for decoding	$[5, 10]$Mb
ξ_0, the unit-normalizing constant	1
β, the constant parameter	2
ϵ, the energy coefficient parameter	10^{-24}
$\varphi^{\min}$, the minimum semantic fidelity	0.3
η, the step size for updating optimization variables	0.001
∇, the computation error	0.001

simulation setup. Then, we illustrate the numerical results and analysis.

A. Simulation Setup

In the simulations, we consider a scenario with five UAVs, one buoy and one UDC. The flying altitude of UAVs is set as 500 m. The flying area of UAVs is within a circle with the radius of 500 m. The vertical distance h between the sea surface and seabed is set as 200 m. The positions of buoy and UDC are set as (200, 200, 0) m and (200, −200, −200) m, respectively. The offset distance κ influenced by the wind and turbulence is set as 1 m. The hyper-parameters of semantic fidelity are based on experimental fitting, and are set as $\omega_1 = -0.0815$, $\omega_2 = 10.7192$, $\omega_3 = -0.7957$, $\omega_4 = 1.0918$. The frequency of the acoustic signal λ is set as 1 kHz [51]. The maximum data transmission delay $T^{\max}$ is 0.5 sec. The maximum transmission power $P^{\max}$ is 1 W. The maximum computation resource of buoy and UDC $\varrho^{\max}_v = 10^9$ cycles/s and $\varrho^{\max}_u = 10^9$ cycles/s. Other parameters used in the simulations are summarized in Table III.

We evaluate the performance of the proposed algorithms in comparison with the following baseline schemes.

- *Frequency division multiple access (FDMA)-based transmission scheme:* In this scheme, UAVs send their sensing data to the buoy via FDMA transmission in Phase I, while the semantic transmission is based on the proposed scheme during underwater transmission.
- *Compression-based transmission scheme:* In this scheme, UAVs send their sensing data to the buoy via NOMA transmission in Phase I. The buoy then compresses the collected data based on the reconstruction-based data compression (i.e., by a compression ratio). The compressed data is finally transmitted to UDC during underwater transmission.
- *Non-compression scheme:* In this scheme, UAVs send their sensing data to the buoy via NOMA transmission in Phase I. The buoy transmits the collected original data to the UDC without data compression during underwater transmission.
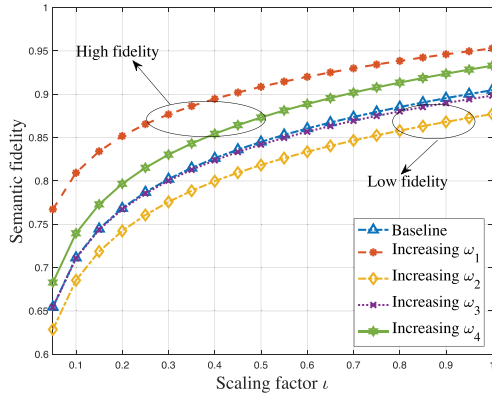
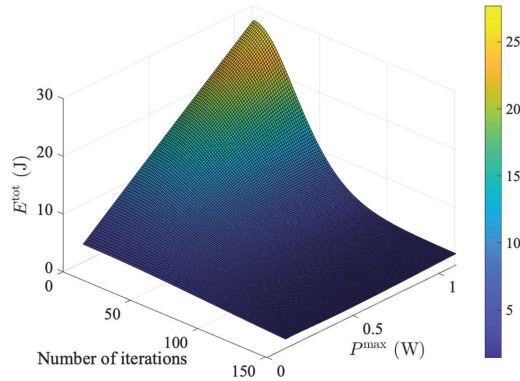Fig. 3. Performance of semantic fidelity with the scaling factor.

Fig. 5. Energy efficiency of the proposed scheme with the number of iterations and average data size.

Fig. 4. Convergence of the proposed algorithm for solving the formulated Problem (SEC).

Fig. 6. Changes of the total energy consumption E^{tot} with the maximum tolerable latency T^{max}.

B. Numerical Results and Analysis

In this subsection, we show simulation results to demonstrate the advantages of the proposed algorithms. Fig. 3 demonstrates the performance of semantic fidelity with the scaling factor ι. It can be seen that the semantic fidelity is positively increasing with the scaling factor ι. By increasing the values of ω_1 and ω_2, we can see that the semantic fidelity is increasing. While increasing the values of ω_3 and ω_4, the semantic fidelity is decreasing. The results show that the scaling factor ι is applicable for semantic information adjustment and can be adjusted flexibly for semantic transmission.

Fig. 4 shows the convergence of the proposed algorithm for solving our formulated Problem (SEC). It can be found that the total energy consumption E^{tot} can converge to a fixed value with the number of iterations. Moreover, the optimal energy consumption is achieved at the feasible value of P^{max}.

Fig. 5 depicts the energy efficiency of the proposed scheme with the number of iterations and the average data size $\tilde{s}_i$. The energy efficiency means the ratio between the throughput and the total energy consumption. It can be seen from Fig. 5 that the energy efficiency tends to converge with the number of iterations, and the lower average data size results in higher energy efficiency because the small data size for transmission will lead to low energy consumption.

Fig. 6 demonstrates the changes of the total energy consumption E^{tot} with the maximum tolerable latency T^{max}. It can
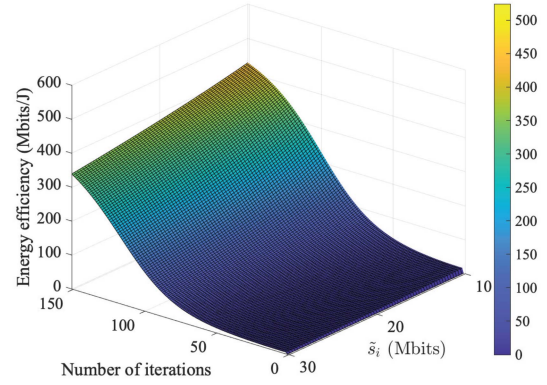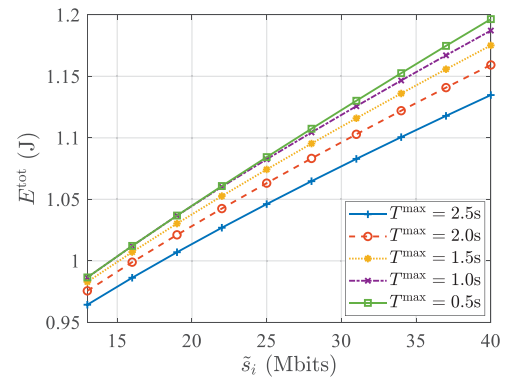
be seen that the total energy consumption E^{tot} is decreasing with the increase of the maximum tolerable latency T^{max}. The reasons can be explained as follows. The high tolerable latency leads to the long transmission durations for UAVs and buoy. The transmission duration is inversely proportional to the energy consumption. Thus, the large tolerable latency results in the low energy consumption. The results also verify the effectiveness of Proposition 1. Moreover, we can find that the system energy consumption is increasing with the average data size. This is because the large data size can increase the transmission consumption, encoding and decoding consumption.

Fig. 7 illustrates the changes of the energy efficiency with the number of iterations. We can obtain from Fig. 7 that the energy efficiency tends to converge as the number of iterations increases. Besides, the high frequency of the acoustic signal λ results in the low energy efficiency. The reason is that the high frequency of the acoustic signal will increase the underwater transmission consumption, which results in the low energy efficiency.

Fig. 8 shows the changes of the energy efficiency with the minimum semantic fidelity φ^{min}. It can be seen that the high semantic fidelity results in the low energy efficiency. The reasons are as follows. The large semantic fidelity can lead to the high workload for semantic transmission, encoding and decoding. This brings high transmission consumption, encoding and decoding consumption, thus increasing the total energy
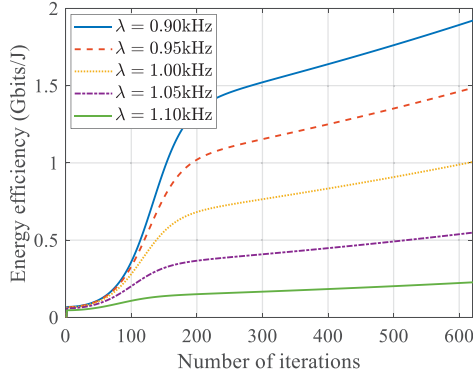
Fig. 7. Changes of the energy efficiency with the number of iterations under different frequencies of acoustic signal.
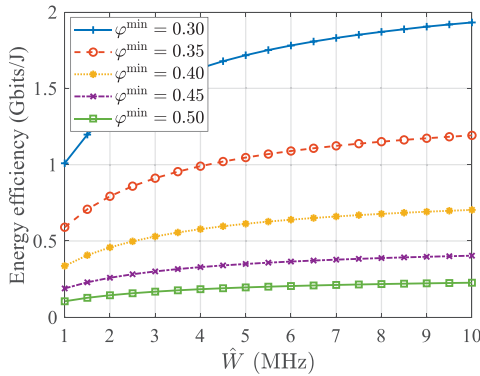

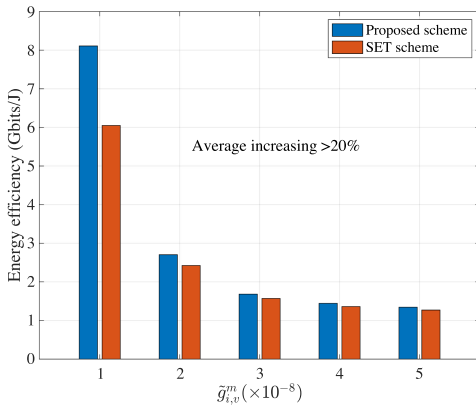Fig. 8. Changes of the energy efficiency with the minimum semantic fidelity $\varphi^{\min}$.

Fig. 9. Comparison of energy efficiency with SET scheme under different values of $\tilde{g}_{i,v}^m$.

Fig. 10. Comparison of energy efficiency with SET scheme under different values of $\tilde{s}_i$.

Fig. 11. Energy comparison of the proposed scheme with benchmark schemes under different frequencies of acoustic signal.

consumption and decreasing the energy efficiency. The results demonstrate the effectiveness of Proposition 1, i.e., the total energy consumption is inversely proportional to the semantic fidelity. Moreover, with the increase of acoustic bandwidth $\hat{W}$, the energy efficiency is increasing. This is because the high acoustic bandwidth can raise the underwater transmission rate, which increases the system throughput and the energy efficiency.

Next, we evaluate the performance of the resource allocation. We compare the proposed scheme with the semantic encoding and transmission (SET) at UAVs. Fig. 9 shows the energy
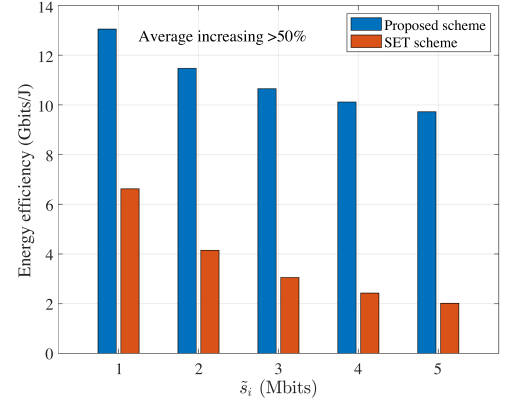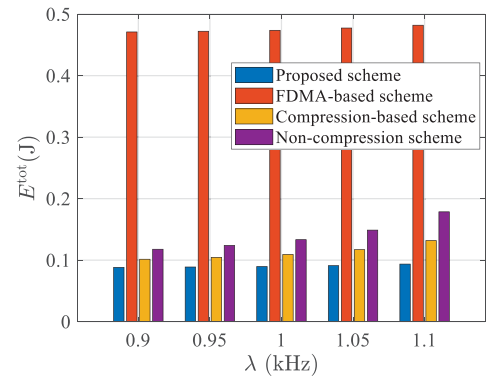
efficiency comparison of the proposed scheme with SET scheme by changing average channel power gain $\tilde{g}_{i,v}^m$. Compared to SET scheme, the energy efficiency of the proposed scheme can be improved by more than 20%. The reason is as follows. In the SET scheme, the semantic encoding and transmission at UAVs lead to high energy consumption, which reduces the energy efficiency.

Fig. 10 depicts the energy efficiency comparison of the proposed scheme with SET scheme by changing average data size $\tilde{s}_i$. It can be seen that the energy efficiency of the proposed scheme outperforms the SET scheme more than 50%. This is because the SET scheme consumes high energy at UAVs, resulting in low energy efficiency. Moreover, as the average data size increases, the energy efficiency in both schemes is decreasing. The reason is that the large data size requires high energy consumption for encoding and transmission.

Fig. 11 demonstrates the energy comparison of the proposed scheme with benchmark schemes under different frequencies of acoustic signal. From Fig. 11, it can be found that the proposed scheme can achieve the lower energy consumption than that of the FDMA-based scheme, the compression-based scheme, and without compression scheme under different values of λ. The reason is as follows. The spectrum utilization in the FDMA-based scheme is low, which increases the transmission consumption. In the compression-based scheme, the compressed data volume is higher than the semantic information, which leads
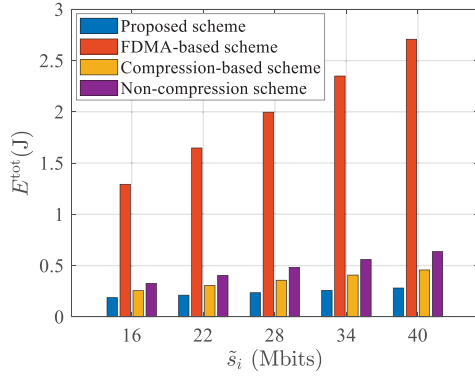
Fig. 12. Energy comparison of the proposed scheme with benchmark schemes under different average data sizes.
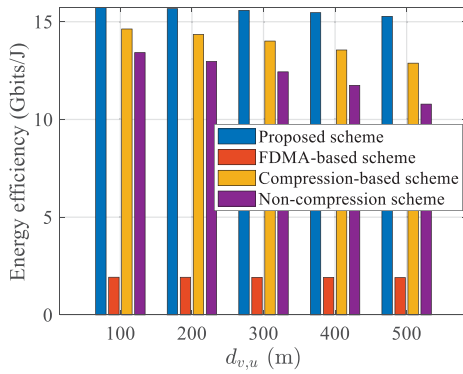

Fig. 14. Comparison of energy efficiency with benchmark schemes under different values of $\tilde{d}_{i,v}$.

Fig. 13. Comparison of energy efficiency with benchmark schemes under different values of $d_{v,u}$.

Fig. 15. Comparison of energy efficiency with underwater bandwidth under different benchmark schemes.

Fig. 16. Comparison of energy efficiency with the number of UAVs under different benchmark schemes.

to the high energy consumption for transmission. As for the non-compression scheme, the original data transmission causes the high energy consumption.

Fig. 12 depicts the energy comparison of the proposed scheme with benchmark schemes under different average data sizes. We can find that the proposed scheme can attain the best performance of energy consumption than the benchmark schemes. Moreover, the energy consumption is increasing with the average data size since the large data size leads to the high energy consumption for data transmission.

Fig. 13 illustrates the comparison of energy efficiency with benchmark schemes under different values of $d_{v,u}$. It can be seen from Fig. 13 that the proposed scheme achieves the best energy efficiency compared to the benchmark schemes. Besides, with the increase of the distance between buoy and UDC, the energy efficiency is decreasing. This is because the long distance between buoy and UDC will lead to high consumption for data transmission, which results in the low energy efficiency.

Fig. 14 shows the comparison of energy efficiency with benchmark schemes under different values of $\tilde{d}_{i,v}$. We can see that the proposed scheme obtains higher energy efficiency than that of benchmark schemes. Moreover, the long distance between UAVs and buoy results in the low energy efficiency since the long distance requires more energy to transmit data, which reduces the energy efficiency.
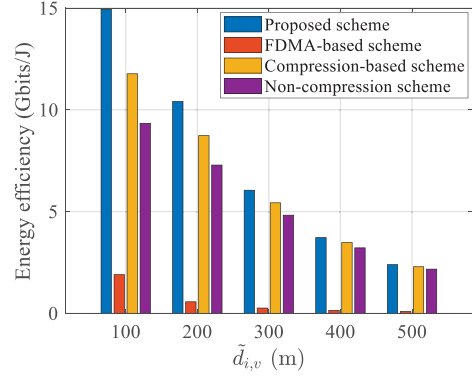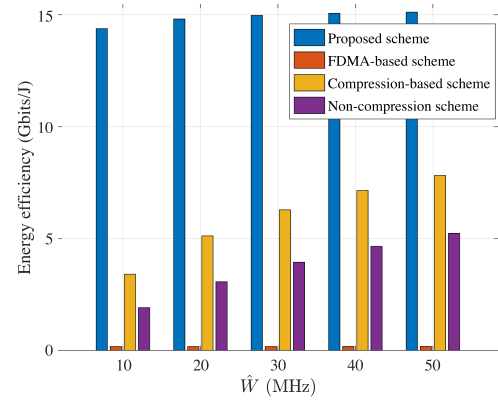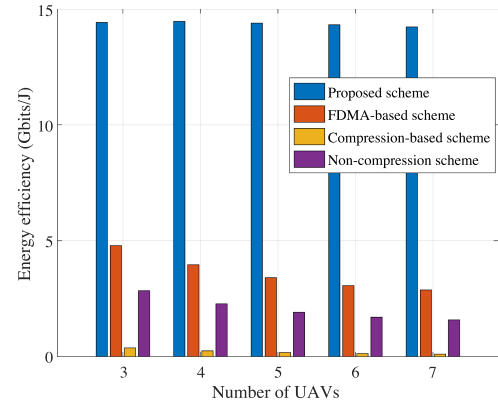
Fig. 15 illustrates the comparison of energy efficiency with underwater bandwidth under different benchmark schemes. It can be seen that the energy efficiency in the proposed scheme is higher than that of benchmark schemes. Moreover, the large underwater bandwidth leads to high energy efficiency because the high value of $\hat{W}$ results in large throughput, which increases the energy efficiency.

In Fig. 16, we test the comparison of energy efficiency with the number of UAVs under different benchmark schemes. We can see that the energy efficiency in the proposed scheme is superior
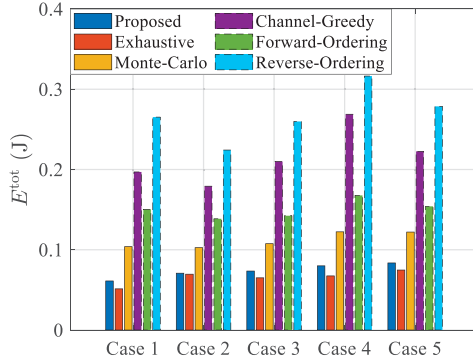
Fig. 17. Energy comparison between the proposed SIC ordering algorithm and heuristic algorithms.
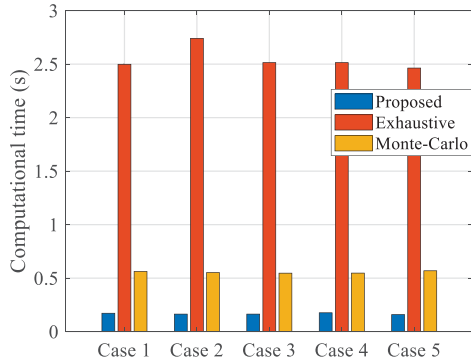

Fig. 18. Computation time comparison between the proposed SIC ordering algorithm and heuristic algorithms.

to other benchmark schemes. Besides, the increasing number of UAVs reduces the energy efficiency because the large number of UAVs causes high energy consumption.

Finally, we compare the SIC ordering algorithm of the proposed NOMA-based transmission with several baseline algorithms including the exhaustive searching algorithm, Monte-Carlo algorithm, channel-greedy algorithm, forward-ordering algorithm and reverse-ordering algorithm. The exhaustive searching algorithm can achieve the global optimality. The channel greedy algorithm means the worse channel will be first decoded. The forward-ordering algorithm means that the channel is decoded by the sequential order. The reverse-ordering algorithm means that the channel is decoded by the reverse order.

Fig. 17 depicts the energy comparison between the proposed SIC ordering algorithm and heuristic algorithms under different cases. The different cases express the parameter changes in different algorithms. It can be seen that the energy consumption of the proposed SIC ordering algorithm is lower than that of the heuristic algorithms, and our design can attain the sub-optimality close to the exhaustive searching algorithm, which validates the effectiveness of the proposed algorithm.

Fig. 18 shows the computation time comparison between the proposed SIC ordering algorithm and heuristic algorithms under different cases. We can find that the proposed SIC ordering algorithm can attain lower computation time than other heuristic algorithms, which validates the efficiency of the proposed algorithm.

VI. CONCLUSION

In this paper, we have proposed a hybrid semantic data transmission framework in air-ocean integrated networks to enhance the data collection efficiency and the reliability of data transmission, with the goal of minimizing the system energy consumption. We considered two transmission layers in which multiple UAVs sense ocean environment and send data to the buoy via NOMA in surface layer, and the buoy uploads the collected data to UDC via acoustic semantic transmission in underwater layer. To improve the reliability of underwater transmission and the acoustic channel utilization, the semantic fidelity is utilized for data transmission with high efficiency. We formulated a resource allocation problem to jointly optimize the semantic scaling factor, the NOMA decoding order, the transmission power and the computing resource allocation. We proposed efficient algorithms to obtain the optimal resource allocations. Simulation results have demonstrated the efficiency of the proposed algorithms compared to baseline schemes. In the future work, we plan to investigate the trajectory designs of the UAVs and buoys which can dynamically move to collect the ocean information of interests and then offload the collected data to the UDC for processing.

REFERENCES

[1] J. A. Zhang et al., "Enabling joint communication and radar sensing in mobile networks—A survey," *IEEE Commun. Surv. Tut.*, vol. 24, no. 1, pp. 306–345, First Quarter, 2022.

[2] F. Peng, Z. Jiang, S. Zhou, Z. Niu, and S. Zhang, "Sensing and communication co-design for status update in multiaccess wireless networks," *IEEE Trans. Mobile Comput.*, vol. 22, no. 3, pp. 1779–1792, Mar. 2023.

[3] F. S. Alqurashi, A. Trichili, N. Saeed, B. S. Ooi, and M.-S. Alouini, "Maritime communications: A survey on enabling technologies, opportunities, and challenges," *IEEE Internet Things J.*, vol. 10, no. 4, pp. 3525–3547, Feb. 2023.

[4] M. Jahanbakht, W. Xiang, L. Hanzo, and M. Rahimi Azghadi, "Internet of Underwater Things and big marine data analytics—A comprehensive survey," *IEEE Commun. Surv. Tut.*, vol. 23, no. 2, pp. 904–956, Second Quarter, 2021.

[5] J. Wang, S. Liu, W. Shi, G. Han, and S. Yan, "A multi-AUV collaborative ocean data collection method based on LG-DQN and data value," *IEEE Internet Things J.*, vol. 11, no. 5, pp. 9086–9106, Mar. 2024.

[6] M. Dai, Y. Wu, L. Qian, Z. Su, B. Lin, and N. Chen, "UAV-assisted multi-access computation offloading via hybrid NOMA and FDMA in marine networks," *IEEE Trans. Netw. Sci. Eng.*, vol. 10, no. 1, pp. 113–127, Jan./Feb. 2023.

[7] Y. Wang, W. Feng, J. Wang, and T. Q. S. Quek, "Hybrid satellite-UAV-terrestrial networks for 6G ubiquitous coverage: A maritime communications perspective," *IEEE J. Sel. Areas Commun.*, vol. 39, no. 11, pp. 3475–3490, Nov. 2021.

[8] Y. Luo, L. Pu, H. Mo, Y. Zhu, Z. Peng, and J.-H. Cui, "Receiver-initiated spectrum management for underwater cognitive acoustic network," *IEEE Trans. Mobile Comput.*, vol. 16, no. 1, pp. 198–212, Jan. 2017.

[9] L. Zhou, S. Leng, Q. Wang, and Q. Liu, "Integrated sensing and communication in UAV swarms for cooperative multiple targets tracking," *IEEE Trans. Mobile Comput.*, vol. 22, no. 11, pp. 6526–6542, Nov. 2023.

[10] M. Dai, N. Huang, Y. Wu, J. Gao, and Z. Su, "Unmanned-aerial-vehicle-assisted wireless networks: Advancements, challenges, and solutions," *IEEE Internet Things J.*, vol. 10, no. 5, pp. 4117–4147, Mar. 2023.

[11] F. Xiong et al., "Energy-saving data aggregation for multi-UAV system," *IEEE Trans. Veh. Technol*, vol. 69, no. 8, pp. 9002–9016, Aug. 2020.

[12] Y. Luo, L. Pu, M. Zuba, Z. Peng, and J.-H. Cui, "Challenges and opportunities of underwater cognitive acoustic networks," *IEEE Trans. Emerg. Topics Comput.*, vol. 2, no. 2, pp. 198–211, Jun. 2014.

[13] X. Zhong, F. Ji, F. Chen, Q. Guan, and H. Yu, "A new acoustic channel interference model for 3-D underwater acoustic sensor networks and throughput analysis," *IEEE Internet Things J.*, vol. 7, no. 10, pp. 9930–9942, Oct. 2020.

[14] S. E. Trevlakis, N. Pappas, and A.-A. A. Boulogeorgos, "Toward natively intelligent semantic communications and networking," *IEEE Open J. Commun. Soc.*, vol. 5, pp. 1486–1503, 2024.

[15] M. Dai et al., "Latency minimization oriented hybrid offshore and aerial-based multi-access computation offloading for marine communication networks," *IEEE Trans. Commun.*, vol. 71, no. 11, pp. 6482–6498, 2023.

[16] S. Meng et al., "Semantics-empowered space-air-ground-sea integrated network: New paradigm, frameworks, and challenges," 2024, *arXiv:2402.14297*.

[17] Z. Li, J. Wen, J. Yang, J. He, T. Ni, and Y. Li, "Energy-efficient space-air-ground-ocean-integrated network based on intelligent autonomous underwater glider," *IEEE Internet Things J.*, vol. 10, no. 11, pp. 9329–9341, Jun. 2023.

[18] N. Z. Zenia, M. S. Kaiser, M. Mahmud, M. R. Ahmed, O. Kaiwartya, and J. Kamruzzaman, "REER-H: A reliable energy efficient routing protocol for maritime intelligent transportation systems," *IEEE Trans. Intell. Transp. Syst.*, vol. 24, no. 12, pp. 13 654–13 669, Dec. 2023.

[19] T. Lyu, H. Xu, F. Liu, M. Li, L. Li, and Z. Han, "Computing offloading and resource allocation of NOMA-based UAV emergency communication in marine Internet of Things," *IEEE Internet Things J.*, vol. 11, no. 9, pp. 15 571–15 586, May 2024.

[20] C. Zeng, J.-B. Wang, C. Ding, H. Zhang, M. Lin, and J. Cheng, "Joint optimization of trajectory and communication resource allocation for unmanned surface vehicle enabled maritime wireless networks," *IEEE Trans. Commun.*, vol. 69, no. 12, pp. 8100–8115, Dec. 2021.

[21] C. Hu, Y. Pu, F. Yang, R. Zhao, A. Alrawais, and T. Xiang, "Secure and efficient data collection and storage of IoT in smart ocean," *IEEE Internet Things J.*, vol. 7, no. 10, pp. 9980–9994, Oct. 2020.

[22] G. Han, A. Gong, H. Wang, M. Martínez-García, and Y. Peng, "Multi-AUV collaborative data collection algorithm based on Q-learning in underwater acoustic sensor networks," *IEEE Trans. Veh. Technol*, vol. 70, no. 9, pp. 9294–9305, Sep. 2021.

[23] J. Wen, J. Yang, W. Wei, and Z. Lv, "Intelligent multi-AUG ocean data collection scheme in maritime wireless communication network," *IEEE Trans. Netw. Sci. Eng.*, vol. 9, no. 5, pp. 3067–3079, Sep./Oct., 2022.

[24] Y. Qian, H. Su, G. Han, J. Zhang, and J. Liu, "Ecologically friendly full-duplex data transmission scheme for underwater acoustic sensor networks," *IEEE Internet Things J.*, vol. 8, no. 9, pp. 7676–7690, May 2021.

[25] S. Kadam and D. I. Kim, "Knowledge-aware semantic communication system design and data allocation," *IEEE Trans. Veh. Technol*, vol. 73, no. 4, pp. 5755–5769, Apr. 2024.

[26] X. Mu, Y. Liu, L. Guo, and N. Al-Dhahir, "Heterogeneous semantic and bit communications: A semi-NOMA scheme," *IEEE J. Sel. Areas Commun.*, vol. 41, no. 1, pp. 155–169, Jan. 2023.

[27] M. Cheng, Q. Guan, Q. Wang, F. Ji, and T. Q. S. Quek, "FER-restricted AUV-relaying data collection in underwater acoustic sensor networks," *IEEE Trans. Wireless Commun.*, vol. 22, no. 12, pp. 9131–9142, Dec. 2023.

[28] Z. Liu, X. Meng, Y. Liu, Y. Yang, and Y. Wang, "AUV-aided hybrid data collection scheme based on value of information for Internet of Underwater Things," *IEEE Internet Things J.*, vol. 9, no. 9, pp. 6944–6955, May 2022.

[29] N. Su, J.-B. Wang, C. Zeng, H. Zhang, M. Lin, and G. Y. Li, "Unmanned-surface-vehicle-aided maritime data collection using deep reinforcement learning," *IEEE Internet Things J.*, vol. 9, no. 20, pp. 19 773–19 786, Oct. 2022.

[30] J. Mcmahon and E. Plaku, "Autonomous data collection with dynamic goals and communication constraints for marine vehicles," *IEEE Trans. Autom. Sci. Eng.*, vol. 20, no. 3, pp. 1607–1620, Jul. 2023.

[31] L. Zong, H. Wang, and G. Luo, "Transmission control over satellite network for marine environmental monitoring system," *IEEE Trans. Intell. Transp. Syst.*, vol. 23, no. 10, pp. 19 668–19 675, Oct. 2022.

[32] L. Lyu et al., "AoI-aware co-design of cooperative transmission and state estimation for marine IoT systems," *IEEE Internet Things J.*, vol. 8, no. 10, pp. 7889–7901, May 2021.

[33] C. Singhal and S. De, *Resource Allocation in Next-Generation Broadband Wireless Access Networks*. Hershey, PA, USA: IGI Global, 2017.

[34] H. Zhang, S. Shao, M. Tao, X. Bi, and K. B. Letaief, "Deep learning-enabled semantic communication systems with task-unaware transmitter and dynamic data," *IEEE J. Sel. Areas Commun.*, vol. 41, no. 1, pp. 170–185, Jan. 2023.

[35] N. C. Luong, T. Le Van, S. Feng, H. Du, D. Niyato, and D. I. Kim, "Edge computing for metaverse: Incentive mechanism versus semantic communication," *IEEE Trans. Mobile Comput.*, vol. 23, no. 5, pp. 6196–6211, May 2024.

[36] A. Li, X. Liu, G. Wang, and P. Zhang, "Domain knowledge driven semantic communication for image transmission over wireless channels," *IEEE Wireless Commun. Lett.*, vol. 12, no. 1, pp. 55–59, Jan. 2023.

[37] Z. Yang, M. Chen, Z. Zhang, and C. Huang, "Energy efficient semantic communication over wireless networks with rate splitting," *IEEE J. Sel. Areas Commun.*, vol. 41, no. 5, pp. 1484–1495, May 2023.

[38] G. Zhang, Q. Hu, Y. Cai, and G. Yu, "Alleviating distortion accumulation in multi-hop semantic communication," *IEEE Commun. Lett.*, vol. 28, no. 2, pp. 308–312, Feb. 2024.

[39] W. C. Ng, W. Y. B. Lim, Z. Xiong, D. Niyato, X. S. Shen, and C. Miao, "Distributionally robust cost minimized edge semantic intelligence in the sustainable metaverse," *IEEE Trans. Mobile Comput.*, vol. 23, no. 7, pp. 7910–7926, Jul. 2024.

[40] Y. He, G. Yu, and Y. Cai, "Rate-adaptive coding mechanism for semantic communications with multi-modal data," *IEEE Trans. Commun.*, vol. 72, no. 3, pp. 1385–1400, Mar. 2024.

[41] X. Pu, T. Lei, W. Wen, and Q. Chen, "Enhancing communication efficiency of semantic transmission via joint processing technique," *IEEE Commun. Lett.*, vol. 28, no. 3, pp. 657–661, Mar. 2024.

[42] C. Liu, C. Guo, Y. Yang, and N. Jiang, "Adaptable semantic compression and resource allocation for task-oriented communications," *IEEE Trans. Cogn. Commun. Netw.*, vol. 10, no. 3, pp. 769–782, Jun. 2024.

[43] D. Tse and P. Viswanath, *Fundamentals of Wireless Communication*. Cambridge, U.K.: Cambridge Univ. Press, 2005.

[44] B. Tang, L. Huang, Q. Li, A. Pandharipande, and X. Ge, "Cooperative semantic communication with on-demand semantic forwarding," *IEEE Open J. Commun. Soc.*, vol. 5, pp. 349–363, 2024.

[45] L. Wang, W. Wu, F. Zhou, Z. Yang, Z. Qin, and Q. Wu, "Adaptive resource allocation for semantic communication networks," *IEEE Trans. Commun.*, vol. 72, no. 11, pp. 6900–6916, Nov. 2024.

[46] Z. Chen, W. Yi, H. Shin, and A. Nallanathan, "Adaptive model pruning for communication and computation efficient wireless federated learning," *IEEE Trans. Wireless Commun.*, vol. 23, no. 7, pp. 7582–7598, Jul. 2024.

[47] P. Li, H. Dong, L. Qian, S. Zhou, and Y. Wu, "FlexGen: Efficient on-demand generative AI service with flexible diffusion model in mobile edge networks," *IEEE Trans. Cogn. Commun. Netw.*, early access, Dec. 23, 2024, doi: 10.1109/TCCN.2024.3522084.

[48] D. E. Lucani, M. Medard, and M. Stojanovic, "Underwater acoustic networks: Channel models and network coding based lower bound to transmission power for multicast," *IEEE J. Sel. Areas Commun.*, vol. 26, no. 9, pp. 1708–1719, 2008.

[49] M. Stojanovic, "On the relationship between capacity and distance in an underwater acoustic communication channel," *ACM SIGMOBILE Mobile Comput. Commun. Rev.*, vol. 11, no. 4, pp. 34–43, 2007.

[50] N. Srinidhi, T. Datta, A. Chockalingam, and B. S. Rajan, "Layered tabu search algorithm for large-MIMO detection and a lower bound on ML performance," *IEEE Trans. Commun.*, vol. 59, no. 11, pp. 2955–2963, Nov. 2011.

[51] R. Ma, R. Wang, G. Liu, W. Meng, and X. Liu, "UAV-aided cooperative data collection scheme for ocean monitoring networks," *IEEE Internet Things J.*, vol. 8, no. 17, pp. 13 222–13 236, Sep. 2021.

Minghui Dai received the PhD degree from Shanghai University, Shanghai, China, in 2021. He is currently an assistant professor with the School of Computer Science and Technology, Donghua University, Shanghai, China. His research interests are in the general area of wireless network architecture and vehicular networks.

Tianshun Wang received the BSc degree in communication engineering from Jilin University, Changchun, China, in 2020 and the PhD degree in computer science from the University of Macau, Macau, China, in 2023. He is currently an assistant professor with the School of Communication and Information Engineering, Nanjing University of Posts and Telecommunications, Nanjing, China. His research interests include mobile edge computing, federated learning, physical layer security, and nonorthogonal multiple access.

Zhou Su (Senior Member, IEEE) received the PhD degree from Waseda University, Tokyo, Japan, in 2003. He has published technical papers, including top journals and top conferences, such as *IEEE Journal on Selected Areas in Communications*, *IEEE Transactions on Information Forensics and Security*, *IEEE Transactions on Dependable and Secure Computing*, *IEEE Transactions on Mobile Computing*, *IEEE/ACM Transactions on Networking*, and Infocom. His research interests include multimedia communication, wireless communication, and network traffic. He received the Best Paper Award of International Conference IEEE ICC2020, IEEE BigdataSE2019, and IEEE CyberSciTech 2017. He is an associate editor of *IEEE Internet of Things Journal*, *IEEE Open Journal of Computer Society*, and *IET Communications*.

Shan Chang (Member, IEEE) received the PhD degree in computer software and theory from Xi'an Jiaotong University, Xi'an, China, in 2012. From 2009 to 2010, she was a visiting scholar with the Department of Computer Science and Engineering, Hong Kong University of Science and Technology, Hong Kong. She was also a visiting scholar with BBCR Research Lab, University of Waterloo, Waterloo, ON, Canada, from 2010 to 2011. She is currently a professor with the Department of Computer Science and Technology, Donghua University, Shanghai, China. Her research interests include security and privacy in mobile networks and sensor networks. She is a member of IEEE Computer Society, Communication Society, and Vehicular Technology Society.

Yuan Wu (Senior Member, IEEE) received the PhD degree in electronic and computer engineering from the Hong Kong University of Science and Technology in 2010. He is currently an associate professor with the State Key Laboratory of Internet of Things for Smart City, University of Macau and also with the Department of Computer and Information Science, University of Macau. His research interests include resource management for wireless networks, green communications and computing, mobile edge computing and edge intelligence. He was a recipient of the Best Paper Award from the IEEE International Conference on Communications in 2016, and the Best Paper Award from IEEE Technical Committee on Green Communications and Computing in 2017. He is currently on the Editorial Boards of *IEEE Transactions on Vehicular Technology*, *IEEE Transactions on Network Science and Engineering*, *IEEE Internet of Things Journal*, and *IEEE Open Journal of the Communications Society*.